Investigation on the Effects of Fastening Parameters on the Handle Displacement of a Pistol Grip Tool

by

Raj Arjun Srinivaasappa Indira

A thesis

presented to the University of Waterloo

in fulfillment of the

thesis requirement for the degree of

Master of Applied Science

in

Mechanical and Mechatronics Engineering

Waterloo, Ontario, Canada, 2022

Author's Declaration

I hereby declare that I am the sole author of this thesis. This is a true copy of the thesis, including any required final revisions, as accepted by my examiners.

I understand that my thesis may be made electronically available to the public.

Abstract

Workers in automotive assembly lines routinely use DC-powered pistol grip tools to install threaded fasteners. While these tools are easy to use and increase production quality, tool operators are subjected to impulsive reaction torques that produce forceful rotary displacement of the tool handle. While operators try to resist this reaction, forces exerted by the forearm muscles are often insufficient, thereby producing eccentric contractions. Repeated exposure to such forces is known to cause tendonitis, fatigue, and physical stress. The objective of this study was to investigate the operational parameters and optimize conditions that minimize the tool handle displacement.

A deterministic approach was considered to identify the system parameters. The tool-operator system was mathematically represented using a single degree-of-freedom torsional model. An *in-vivo* study of 10 experienced workers was conducted to estimate the typical ranges of operator stiffness. Tightening tasks were performed at 3 torques (5, 7.5, 10 Nm), and 4 fastener locations that correspond to varying orientations of the wrist. The mean operator stiffness was found to be 1.11 kN/m. A pistol grip tool simulator was designed and developed to emulate the dynamics of tightening operation without the use of human operators. A slider-crank mechanism was considered to represent the kinematics of the torsional system, and a pneumatic actuator was used to represent individual operator stiffness.

A parametric study observed the effects on tool handle response due to varying torque, operator stiffness, spindle speed, fastener material, drive style, and fastener head type. Results showed that an increase in applied torque (5–7.5 Nm) also increased the angular displacement of the tool handle (42.2°–58.5°). Variation in stiffness resulted in an inverse effect on the handle response. At 7.5 Nm, it was observed that wrist ulnar deviation produced the most handle displacement (59.2°), whereas wrist flexion produced the least (57.3°). Variation in the operational speed of tool spindle showed no significant effect on the handle displacement. Three fastener materials, alloy steel, stainless steel, and brass were tested. It was observed that alloy steel resulted in the least displacement (65.4°), whereas brass produced the most (85.7°). Between the two drive styles, it was observed that a Hex drive produced significantly higher response (69.9°) than a Torx Plus drive (63.4°). Button Head fasteners produced significantly higher response (76.2°) compared to Flat Head fasteners (66.9°). Based on this data, it was concluded that the designed pistol grip tool simulator can be used to investigate and optimize the operational parameters such as tool tightening algorithm, fastener types, and task locations, thus minimizing the tool handle displacement and mitigating forearm strain injuries.

Acknowledgements

First and foremost, I would like to thank my supervisor Dr. Naveen Chandrashekar for providing me with this opportunity to pursue my master's research, and for his constant support and guidance throughout this journey. I would like to thank the industrial partner, Honda of Canada Manufacturing (HCM), Alliston, ON and its workers for their participation and feedback. I would like to extend my thanks to Tom Gawel for his valuable help with conducting experiments. I also thank Dan Loewen and Brendan Pinto for helping me complete the in-vivo study at HCM.

I appreciate the constant support provided by my fellow lab mates Pratishtha Gupta, Mercy Ombogo and Harish Rao, and for being the first test subjects of this study. Lastly, I also thank my family and friends for always encouraging me to do better. I couldn't have done this without you all.

Table of Contents

List of Figures

List of Tables

Chapter 1

Introduction

1.1 Motivation

Workers in the manufacturing assembly line at Honda of Canada Manufacturing (HCM), Alliston, Ontario, routinely use hand-held DC-powered torque tools to install threaded fasteners. Among several hand-held torque tools, pistol grip tool configurations have become increasingly popular. Over the years, these tools have contributed to significant improvements in terms of product quality assurance, accuracy, and productivity. While these tools are easy to use and have increased production quality, the tool operators are subjected to impulsive handle reaction forces when the tool torque builds up during the tightening phase. These reaction forces, commonly known as 'kickbacks', result in forceful rotary displacement of the tool handle. The operator thereby needs to oppose these forces by limiting the displacement of the tool handle but are often incapable. Repeated exposure to such forces is known to cause repetitive strain injuries (RSIs). Workers have been diagnosed with RSI related to wrist, hand, and forearm for several years now. Whenever medical intervention is required, each of these injuries cost as much as $60,000 to the company. Therefore, it is crucial to minimize the tool handle displacement during pistol grip tool operation.

Several studies have tried to address the relevant issue, but none of the published data could be used to study the parameters that affect the handle displacement of the pistol grip tool that HCM needs it to be studied. This is because the handle displacement is specific to each operator, location, and task specifications. For example, workers assume different positions to tighten fasteners that are at different heights on the chassis of a car. Therefore, it is required to model the variation in positions as well as other relevant parameters. Further, DC-powered tools allow a great deal of flexibility in tightening parameters, such as the target torque, spindle speed, torque input profiles, and tightening strategies. These parameters are known to have an impact on the dynamic interaction between the tool and the operator. Therefore, it is crucial to estimate the ergonomic impact of various tool settings and fastener design specifications.

It is difficult to test the effects of these various parameters directly on human subjects due to variability and ethical concerns. Therefore, these parameters can only be investigated experimentally with a test rig that simulates the tool dynamics. Once these parameters are investigated, they can be optimized to minimize the handle displacement caused due to the reaction torque.

1.2 Objectives

The primary objective of this study was to test the effects of various tightening parameters on the handle displacement during pistol grip tool operation. The specific objectives were:

1. Model the dynamic interaction between the pistol grip tool and operator using a single degree-of-freedom mechanical torsional model and use in-vivo experimental data to estimate the model parameters.
2. Design and develop a pistol grip tool simulator that emulates the dynamics of tightening operation by incorporating the model parameters.
3. Investigate the effects of tightening parameters related to tool, task, and operator, and establish the optimum conditions required to minimize the tool handle displacement.

1.3 Thesis Overview

This thesis is organized into six chapters. Chapter 1 (Introduction) describes the relevant issue upon which this research is conducted. Chapter 2 (Background) introduces the anatomy of the human hand and forearm, the various types of torque tools currently in use, hand-arm injuries associated with torque tool usage, and previous research literature. Chapter 3 (Methodology) consists of three main sections. The first section describes the analytical model of the tool-operator dynamic system. The second section summarizes the in-vivo study conducted to estimate the operator characteristics. The third section includes the design and development of the pistol grip tool simulator. Chapter 4 (Results) presents all the results of this study, including the performance evaluation of the tool simulator and its parametric study. Chapter 5 (Discussion) investigates the results of the current research in comparison with previous studies, as well as its novel findings. Chapter 6 (Conclusion) presents the conclusions of this study, its limitations, as well as recommendations for future work.

Chapter 2

Background

2.1 Anatomical Background

Investigating the mechanisms behind power tool injuries requires a comprehensive understanding of the human body anatomy. This entails defining the nomenclature used to describe the positions, movements, and orientations of different parts of the body. This section summarizes the anatomical background required to study the biomechanical interaction between power tools and the human hand-arm.

2.1.1 Nomenclature

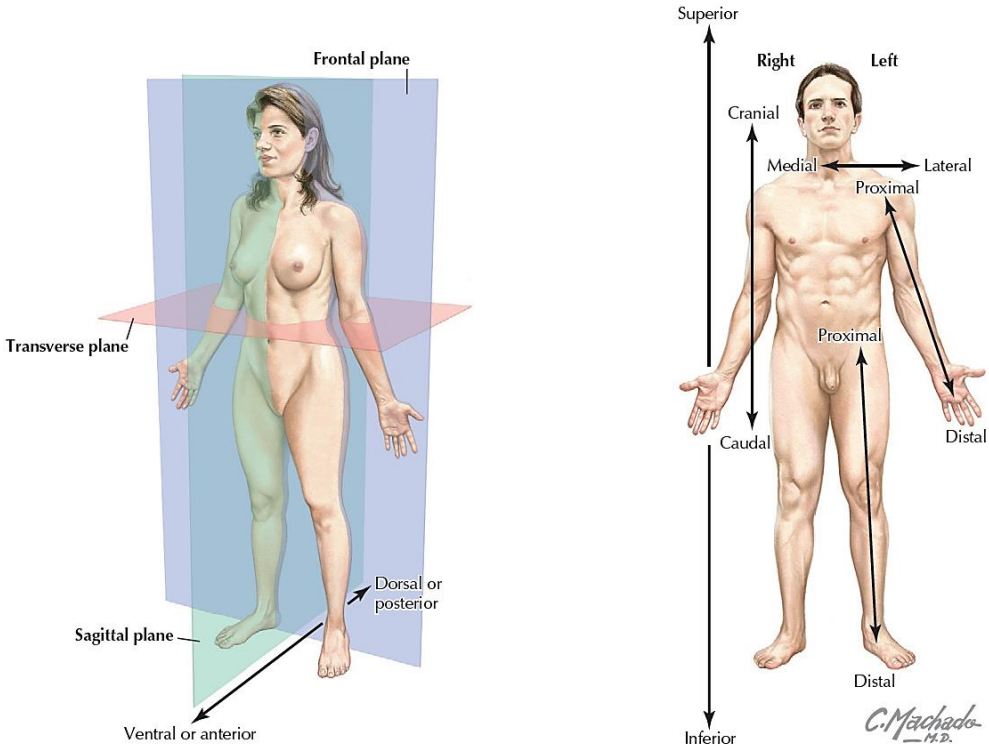

Figure 2.1: Anatomical planes of the human body (Hansen, 2014)

Body Planes

Anatomically, the human body is sectioned into three orthogonal planes, as shown in Figure 2.1. The sagittal (longitudinal) plane divides the body into left and right (medial and lateral). The frontal (coronal) plane divides the body into front and back (anterior and posterior). The transverse (axial) plane divides the body into head and torso (superior and inferior).

Movements

Body movements primarily occur due to the articulation provided by joints where two or more bones or cartilages meet. Muscles are responsible for performing these movements through myoelectric signals from the brain. For example, in the context of hand tool usage, the forearm muscles are responsible for the movements of the wrist joint. The three primary movements of the wrist are shown in Figure 2.2.

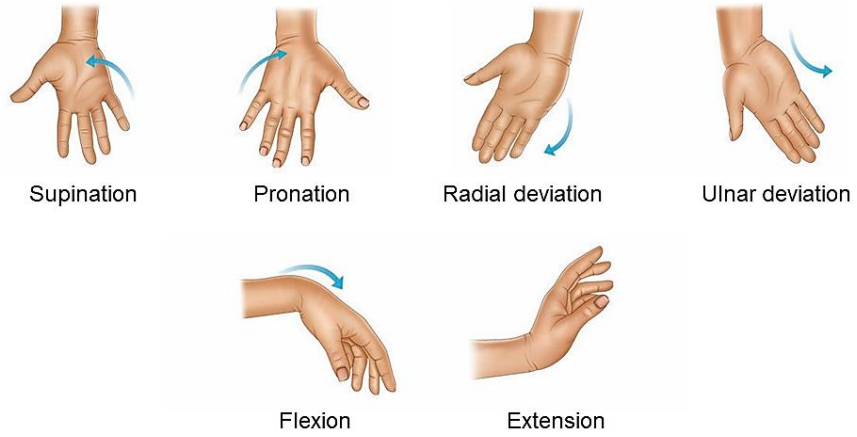

Figure 2.2: Movements of the wrist (© Health Books UK Ltd., 2021)

The range of movement of the wrist varies with each person and is generally measured using a goniometer. The typical range of movement of the wrist for flexion-extension is 60°, radial deviation is 20°, and ulnar deviation is 30° (Pillemer, 2022).

2.1.2 Forearm and Hand

The forearm and hand are two among the four sections of the upper limb. The region between the elbow and wrist joints is considered the forearm. It consists of two bones namely, radius and ulna. The forearm muscles are mainly classified as flexors and extensors, each responsible for different set of wrist movements. The primary muscles involved in wrist flexion are the flexor carpi radialis (FCR), and the flexor carpi ulnaris (FCU). Secondary muscles include palmaris longus, and flexors of the digits (fingers). The primary muscles involved in wrist extension are the extensor carpi radialis longus (ECRL), and the extensor carpi radialis brevis (ECRB). Secondary muscles include extensors of the digits. Radial deviation (abduction) is performed by the flexor carpi radialis, and extensor carpi radialis longus and brevis muscles acting simultaneously. Ulnar deviation (adduction) is performed by the flexor carpi ulnaris and extensor carpi ulnaris muscles acting simultaneously. The muscles involved in wrist pronation are the pronator teres, pronator quadratus, and brachioradialis. The muscles involved in wrist supination are the supinator and biceps brachii. The anatomy of the forearm muscles is shown in Figure 2.3.

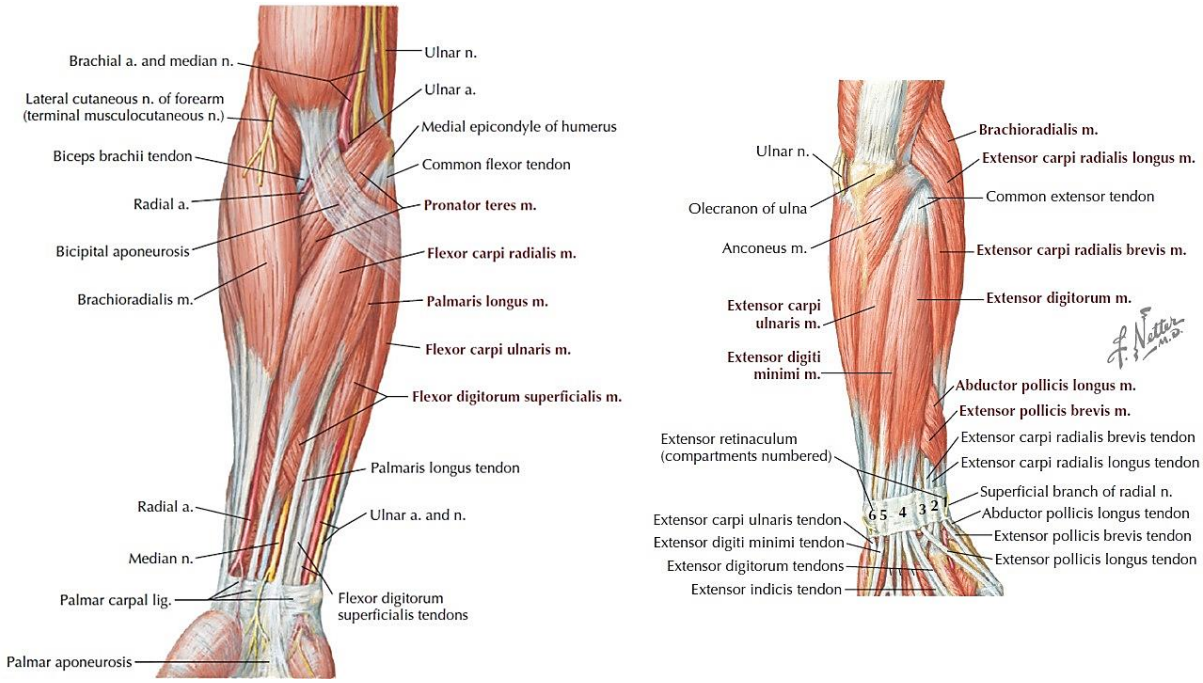

Figure 2.3: Anatomy of forearm muscles (Hansen, 2014)

On the distal end of the forearm, the wrist joint connects to the hand. The wrist consists of eight carpal bones which lie in two rows. The hand consists of five metacarpal bones that make the palm, and five phalanges that make the digits. The metacarpophalangeal joints (knuckles) connect each of the five metacarpal bones to their corresponding phalanges, as shown in Figure 2.4.

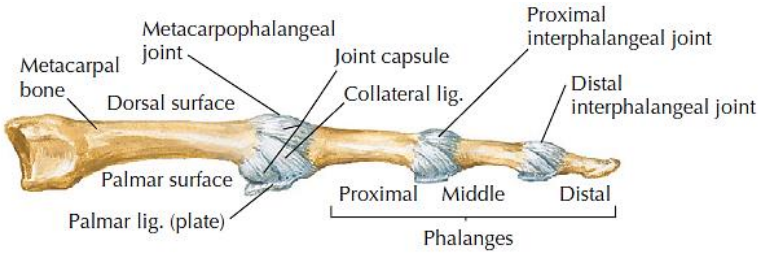

Figure 2.4: Anatomy of hand (Hansen, 2014)

In the use of hand tools, the primary function of the hand is to grip the tool handle. Grip force is produced by the flexor digitorum profundis (FDP), flexor digitorum superficialis (FDS), and flexor pollicis longus (FPL) muscles. Whereas grip relaxation is produced by the extensor digitorum communis (EDC).

2.2 Torque tools

Torque tools are commonly used to tighten fasteners in several manufacturing applications, including automobile, aerospace, naval, and household appliance industries. They have become increasingly popular

in manufacturing assembly lines over the past few decades, owing to their ease of use, increased production output and quality. Several configurations of torque tools are commercially available, while hand-held tools are the most popular. Hand-held torque tools are primarily classified based on their power source, as well as the shape. The most commonly used power sources for torque tools are pneumatic and electric. Pneumatic tools are powered with compressed air, making them less expensive than electric tools. They are also lighter, and safer to use in wet environments. However, pneumatic tools can be disadvantageous as they require a bulky compressed air tank, and require high maintenance due to moisture, rust, and friction. While pneumatic tools were traditionally used, electric tools have become increasingly popular owing to their precisely controllable technology. These tools are driven by DC motors that have their own position encoders and computer controllers. This enables closed-loop control of torque and speed, to accurately apply the desired torque levels as well as control the spindle motion. Electric tools can be either powered by an electric cable or built-in battery, making them extremely portable.

Torque tools are also classified based on their body shape, which vary depending on the application, torque range, and ease of use. Commonly used shapes include right angle (RA), in-line (IL), and pistol grip (PG) configurations, as shown in Figure 2.5. Right angle tools are commonly used owing to their capability of operating at high torques and speeds. They are typically larger in size and heavier than other tool shapes. As the name signifies, the rotational axis of the motor is in right angle with the driver spindle axis. Further, in-line tools are commonly used in applications with small, tight spaces, low torques, and are lightweight. Pistol grip tools embody the best of both right-angle and in-line tools. They are capable of delivering high torques and speeds, are relatively smaller and lightweight. The use of a pistol grip handle makes them highly practical and convenient to use. While the motor is aligned with the driver spindle axis, the tool handle is approximately orthogonal to it, thus reducing the handle reaction during tightening.

Figure 2.5: Torque tool configurations based on body shape (© Atlas Copco)

Modern electric torque tools with advanced controllers are capable of precise measurements of the tool torque and rotation of the spindle. The fastener tightening consists of three phases of operation. The initial phase is called the rundown, where the tool spindle drives the fastener into the threaded component until the torque within the fastener reaches approximately 10% of the target torque (ISO 5393). The next phase is called the torque build-up phase, where the fastener is being driven until it reaches the desired torque level. The end of the torque build-up phase is marked by the peak torque and peak angle of the fastener, as shown in Figure 2.6. The third phase occurs once the tool reaches the peak torque, and the driving motor is shut-off automatically by the controller. Typical torque build-up phase lasts a few hundred milliseconds; however, the actual durations depend on the tool spindle speed (Kihlberg et al., 1993).

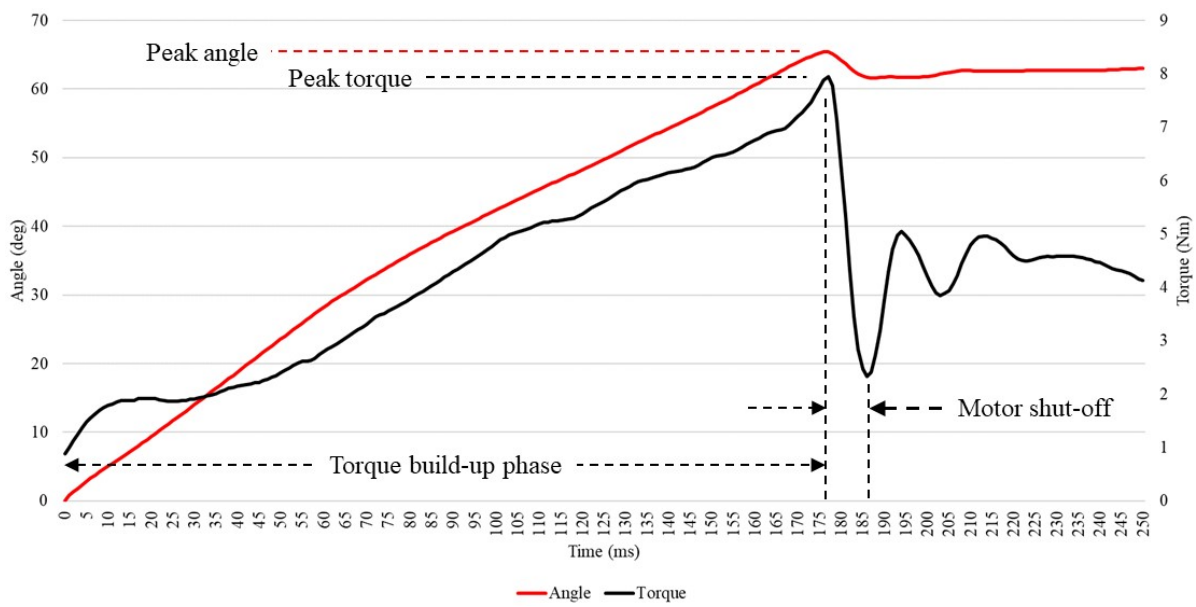

Figure 2.6: Tightening phase of torque and angle measurements

The torque build-up phase also exerts a reaction torque from the fastener against the driving motor, which further translates to a reaction motion of the entire tool body relative to the spindle. Such reaction torques act against the operator holding the tool during tightening. Due to the impulsive, momentary nature of the reaction torque, it is widely known to cause injuries among tool operators.

2.3 Repetitive Strain Injuries

Such injuries that are known to be a result of power tool reactions are commonly known as repetitive strain injuries (RSI) of upper extremity. They are associated, or made worse, by repetitive movements of the tool handle, hand-arm movements outside their normal range of motion, excessive fastener torques, long durations of workload, awkward gripping of tool handle, badly designed or faulty equipment, poor working environments, fatigue, and stress.

Initially, tool operators overcome the tool reaction with a concentric muscle contraction (muscle shortening) (Oh et al., 1997). However, as the torque builds up beyond the capabilities of the operator, it causes a motion against the muscle, producing a forceful eccentric muscle contraction (muscle lengthening), as shown in Figure 2.7. Thus, muscles undergoing such eccentric contractions behave like a spring, producing even more force. Therefore, repeated eccentric contractions of the muscles involved in opposing the tool reaction have negative consequences. Common injuries include carpel tunnel syndrome (Bakker et. al., 2022), tendonitis, lateral epicondylitis (tennis elbow), stenosing tenosynovitis (trigger finger), among many others. Common symptoms of these injuries include muscle damage, muscle soreness, swelling, numbness, restriction of joints, loss of grip strength, and loss of sensation. The severity of these injuries is proportional to the magnitude of the tool torque, spindle speed, and displacement of the tool handle.

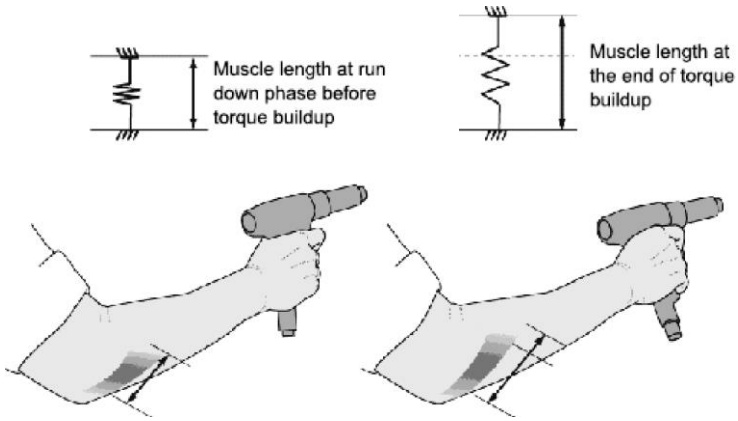

Figure 2.7: Muscle reaction to tool torque build-up (Lin et al., 2003b)

Several surveys have reported the high prevalence of work-related upper extremity injuries among workers in manufacturing industries. Data released from the National Institute for Occupational Safety and Health (NIOSH) stated that workers in automotive manufacturing industries experience an unusually high incidence of repetitive strain injuries (Ay, 2010). Among hand tool-related injuries in the United States, 22% were caused by powered hand tools, primarily due to struck by or struck against and overexertion (Lin, 2010a). Honda of Canada Manufacturing (HCM) reports that most workers in the assembly line of their manufacturing unit use DC hand tools extensively every day to apply variety of torques on different fasteners in various operating positions. Workers have been diagnosed with overuse injuries related to wrist, hand, and forearm for several years; and when medical intervention is needed, each of these injuries cost as much as $60,000 to the company. Therefore, extensive research has been carried out in the past few decades towards mitigating repetitive strain injuries related to torque tool usage. Section 2.3 outlines some of the relevant literature.

2.4 Literature Review

For the current study, more than 50 peer-reviewed research articles were investigated. It was observed that several approaches were used to address the relevant issue, directly and indirectly. Therefore, the approaches (or methods) were filtered and selected based on a relevance criterion. The methods considered for this study were biomechanical analytical models, experimental simulation models, use of actual or prototyped power hand tools, modelling physiological and psychological responses of tool operators, and dynamic interactions between hand-arm and tool interface. Several important reaction parameters were also considered for the criteria, and the potential linkages between reaction parameters and risk of injury was explored. Further, the objectives, experimental design, sampling methods, dependent and independent variables, physiological biometrics such as EMG were also considered. However, some papers were excluded for this study, particularly ones related to vibration exposure and tool handle design as no clear correlations to the current study were identified.

It was observed that all studies investigated the reaction parameters of the operator during power hand tool operation. The most common parameters studied were reaction force/torque, impulse, handle displacement, velocity/acceleration, and some studies also included power and physiological changes. The results of these parameters are discussed in the current section. Further, the values for different reaction parameters are compared and their linkages with the risk of musculoskeletal disorders are mapped out. Furthermore, recommendations for reaction parameters are also outlined to emphasize the current acceptability limits for power hand tool operations.

2.4.1 Analytical Models

Description

Researchers have used simple mechanical systems to model human responses to transient perturbations. In the past, static linear modelling approaches have been used to model the response of an arm in the vicinity of equilibrium position. Specifically, a static stiffness parameter was used to model the arm displacement by applying small displacements to subjects' hands and calculating the static stiffness using linear regression. Lin et al. (2003c) estimated the static handle force needed to support a power nutrunner when it is operated against a tightening fastener with a constant torque. The static force model was a function of the tool geometry, mass, orientation in space, applied torque, torque build-up, and stall torque, and a moment equilibrium equation was used to derive the resultant handle force in matrix form. However, this approach was limited since it was a static model and the inertial and damping effects in hand-arm dynamics were neglected.

Lin et al. (2001) established a novel single degree-of-freedom (DOF) mechanical system that could be used to sufficiently model the hand-arm dynamics while using pistol grip hand tools. The hand and arm, lumped, is represented with stiffness, damping and mass parameters which are dependent on the operator and their posture, as shown in Figure 2.8. Full factorial experiments were conducted on 25 subjects for parameter identification based on gender, horizontal distance, and vertical distance from ankles to the handle. Lin et al. (2003a) further validated this second-order model for various tool shapes - in-line, pistol grip, and right angle. Free-vibration method was used, and the resulting frequency and amplitude of handle response was calculated for opposing the external load using maximum effort. However, these parameters were calculated based on maximum effort by the operator, and therefore do not represent actual tool operation. Lin et al. (2003b) later proposed scaling the stiffness parameter in their previous study with the normalized forearm flexor muscle activity, recorded through electromyography (EMG), to determine the model parameters for actual hand tool operation. The experiment was a repeated-measures (3 replicates) 4×2×2×2 full factorial design, consisting of six power nutrunners operated by 9 subjects (3 men, 6 women) in a laboratory. The EMG data was used to account for the model changes with respect to working posture. Lin et al. (2005) in a later study used the mathematical model to accurately predict operator responses and reaction capacities and presented a selection criterion for the appropriate tool type as well as optimize the workplace design in industrial jobs. They study developed an interpolation method to find the model parameters linearly for varying vertical and horizontal tool locations within a test range, therefore the model could be used for general practical applications.

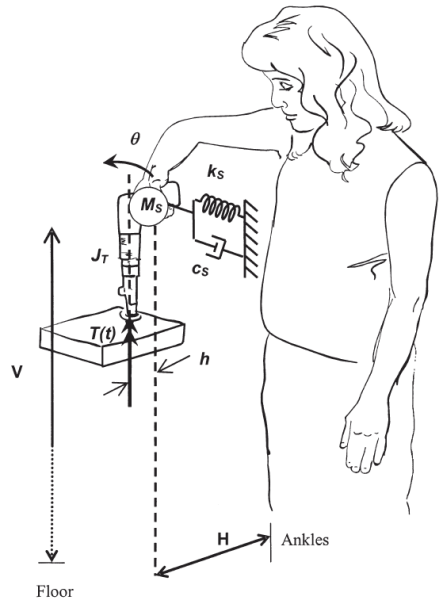

Figure 2.8: Single DOF mathematical model to predict operator responses (Lin et al., 2003b)

Further, Ay et al. (2013) established a new testing protocol for estimating the stiffness, damping and mass parameters in the aforementioned linear dynamic model for right angle (RA) tools. The authors developed a novel testing apparatus which consisted of a prototype actuated by an actual RA tool to closely mimic the operator interactions with an RA tool. Forty experienced tool operators were tested with the apparatus to determine the hand-arm reaction force and peak handle displacement in terms of the input torque and time taken to reach the target torque.

Results

The analytical models outlined in this review primarily tested for the dynamic characteristics, stiffness, damping and mass of the operators. Lin et al. (2001) showed that the torsional stiffness (Nm/rad) changed by 20.6% for vertical distances from 55 to 190 cm, and 23.6% for horizontal distances from 90 to 30 cm. No significant variation in damping was observed, however the mass moment of inertia changed by 44.5% for vertical and 41.2% for horizontal locations. Further, it was found that the mass and damping for males were 31.1 and 38.5% respectively greater than females. Lin et al. (2003a) in a similar study with various tool shapes, validated that the operator linear stiffness decreased from 1721 to 1196 N/m for horizontal locations, and increased for vertical locations. The mass moment of inertia for gender variances also showed a similar trend as the previous study. It also concluded that stiffness was the most significant factor influenced by workplace conditions. Lin et al. (2003b) used EMG to adjust the stiffness values to account for individual differences in working conditions. The model was then used predict the handle displacements and compared them to the measured values. The results showed that the model overpredicted the actual displacements by only 3% (R=0.98). Whereas without the EMG correction, the model overpredicted the actual displacements by 10%. Further, it was shown from the hand forces that females had a more delayed response (214 ms) to reaction forces than males (107 ms). Lin et al. (2005) successfully developed an interpolation model to predict group means of handle displacement and force. For example, a pistol grip nutrunner used at a horizontal distance of 30 cm and vertical distance of 140 cm resulted in a mean handle displacement of 39 mm for males. As a result, 63% of males exceeded a 30 mm displacement limit. Whereas, when a right-angle tool of similar torque is used, only 4.6% of the male users exceeded the 30 mm limit. This allowed for interpolating the reaction parameters at any given work location where the parameters are not available within the test range. The predicted handle displacements and force for 25 operators are tabulated in Table 2.1. Later, Ay et al. (2013) validated Lin's model with a novel testing apparatus and confirmed that the model parameters were significantly affected by working postures and gender.

Table 2.1: Predicted means and SD of handle displacement and hand force (Lin et al., 2005)

Tool	Location	Response	Male Mean	Male SD	Female Mean	Female SD
Right angle tool A on horizontal surface	Far	Disp (mm)	25.4	17.4	27.7	11.6
		Force (N)	36.3	5.8	38.1	6.0
	Near	Disp (mm)	13.8	9.6	17.8	8.8
		Force (N)	36.0	5.5	38.8	4.3
Pistol grip tool B on horizontal surface	Far	Disp (mm)	64.5	27.2	64.8	35.3
		Force (N)	99.2	7.3	102.9	9.0
	Near	Disp (mm)	39.0	28.1	31.5	17.3
		Force (N)	95.0	12.4	91.6	13.6
Pistol grip tool B on vertical surface	Far[A]	Disp (mm)	82.9	28.9	116.7	24.3
		Force (N)	98.2	8.6	90.2	13.6
	Near	Disp (mm)	50.5	21.0	69.6	43.1
		Force (N)	103.2	9.5	100.9	8.0

2.4.2 Physiological and Psychological Measures

Description

As opposed to using mathematical mechanical systems to model the reaction parameters of the operator, several studies have commonly modelled the physiological responses during tool handle reaction. It was observed that the most common biometric used was electromyography (EMG) to measure the muscle activity in the hand-arm. EMG measures the muscle response or electrical activity in response to the external load exposure from tool handle. Kihlberg et al. (1993) measured operator EMG to calculate the force exerted at the operator's hand during tool operation. The study was a repeated measures 3×5 full factorial design with 12 male subjects, and their reaction forces and hand-arm displacement were studied during tightening of threaded fasteners with three nutrunners of the same target torque. The EMG activity was measured in six muscles with surface electrodes and the responses between muscle groups were compared to assess their individual influences on producing the opposing hand force. Similarly, Oh et al. (1997) used EMG to study the effects of reaction force and workplace design on the handle kinematics and operator muscle activity. The tool reaction parameters included the target torque, joint hardness, tool orientation and operator distance. The dependent variables measured were the tool handle kinematics i.e., peak handle velocity and peak handle displacement, and the EMG activity in the forearm and upper arm muscles. Further, the relationship between operator strength and handle kinematics was studied to determine the conditions to minimize tool instability.

Lin et al. (2003b) used normalized EMG of the forearm flexor muscles to measure the muscle exertions during eccentric contractions. The average RMS EMG was normalized to the maximum voluntary contractions and used to proportionally adjust the stiffness values in their mathematical model, hence providing accurate relative exertion levels as opposed to absolute levels. Lin et al. (2007) measured the

handle displacement, grip force and upper limb activity (EMG) to test the effects of operator experience, workplace distances, tool types and joint hardness. The average EMG scaled to reference voluntary contractions (RVC) was compared between 15 experienced and 15 novice nutrunner operators. Lin et al. (2010a), besides using EMG to measure muscle activity, also modelled the grip forces at the tool handle using strain gauges. These physiological responses on upper extremities were measured for 32 right-handed male operators using 4 tools on 2 joint simulators at varying workplace distances. The operator performance was evaluated for torque exposure time, peak torque, reactive hand moment impulse, normalized grip force and integrated EMG at three muscle groups. Similarly, Lin et al. (2012) measured grip force and EMG on 21 men using pneumatic nutrunners for 12 repetitive fastener-driving sessions on 3 joints at slow and fast pace and included two different work-rest ratio patterns. The optimum working conditions and rest break periods were identified to reduce perceived exertions. Forsman et al. (2002) investigated the muscle activity during pneumatic nutrunner usage at a bus assembly plant and characterized the variances in muscular effort using EMG at five muscles. The EMG was measured and compared for soft and hard joints, three joint positions, and two tools. Steingraber et al. (2021) conducted a similar study to assess the handle force and upper extremity kinematics using surface EMG for right angle hand tools at varying locations, orientation, target torque and joint hardness. The study used 36 subjects and tested a rapid and short duration fastening strategy called TurboTight developed by Atlas Copco (largest nutrunner manufacturer), compared to conventional strategies – two-stage (TS) and two-stage with soft stop (TSS).

Lin et al. (2010b) considered a different physiological measure to model the operator capacity to generate opposing forces. Near-infrared spectroscopy (NIRS) was used to monitor the changes in regional tissue oxygenation and blood volume from flexor digitorum superficialis and extensor digitorum communis. The tissue oxygenation index indicated the dynamic balance between oxygen delivery and oxygen consumption in the tissues, and this was compared for different work-rest ratios and paces. McGorry et al. (2009) similarly measured the muscle oxygenation and blood volume in the extensor carpi radialis and the flexor digitorum superficialis during isometric gripping tasks and compared the effects of varying handle diameters. Sesto et al. (2005) conducted a study to investigate the effects of power hand tool use for short durations on the dynamic mechanical properties (stiffness, damping, mass) and edema of the forearm. The repetitive submaximal eccentric exertions in the forearm were modelled for different tool exercise tasks and the edema (muscle water content) was measured using Magnetic Resonance Imaging (MRI). The edema indicated changes in muscle strain and muscle soreness before and after the tasks and was used to evaluate the level of exertion.

Chang et al. (1999) investigated the effects of wearing a glove and wrist support to minimize hand-arm response while operating an in-line pneumatic nutrunner. The hand-arm response was modelled using

triggering finger force and flexor digitorum EMG. Four glove types (barehanded, cotton, nylon, open-finger), and two wrist supports (wearing, not wearing) were tested for 13 male subjects operating one tool on a single horizontal plate. Chang et al. (2000) studied the hand-arm stress induced while operating an electric screwdriver in terms of finger force exertion and EMG. The study tested two activation modes, two target torques and three horizontal distances on 13 male subjects recruited from the previous study. In both studies, finger force was measured using thin film forces sensors taped to the phalangeal pads of individual fingers, and surface EMG electrodes were placed over the flexor digitorum.

Kihlberg et al. (1993) studied the self-reported ratings of discomfort perceived by operators for three different nutrunners. The discomfort was rated with a modified Borg's CR-10 scale, where a rating of 0 indicated nothing at all, and 10 indicated extremely strong (almost max). Similarly, Kihlberg et al. (1994) used the modified Borg's CR-10 scale to rate the perceived operator strength and a similar 20-point scale to rate the level of discomfort (0 – no discomfort at all, 20 – almost unbearable). Kihlberg et al. (1995) used subjective ratings of discomfort of the reaction by 38 subjects. The subjects also answered the question, "Would you accept to work a whole working day with a tool that gives a reaction force like this?". The ratings were then used to find acceptability limits for the discomfort from pneumatic tool reaction forces. Lin et al. (2008) used subjective ratings of discomfort to identify its relationship with tool operation parameters such as work location, grip force and handle displacement. Twenty male subjects were called to operate four pneumatic tools and nine work locations and corresponding subjective ratings were collected. Sesto et al. (2005) administered a self-reported symptom questionnaire which included questions about localized discomfort and upper extremity symptoms such as numbness, pain, tingling and aching. Also, an analog scale ranging from 0 to 10 (0 – no pain, 10 – most pain) was used to assess pain intensity before and after the tasks.

Results

Kihlberg et al. (1993) measured EMG activity in six muscles for different build-up times and found that the fast shut-off tools had smallest values (μV), whereas delayed shut-off tools caused the largest values, as expected. However, the EMG measures showed no consistent response patterns, possibly due to choosing the wrong muscle groups. Regardless, the self-reported discomfort ratings were highly correlated with the target torques, but moderately correlated with reaction torques. Similar trends in ratings were observed in Kihlberg et al. (1994) as well. Kihlberg et al. (1995) reported that no subject would work a whole day with a discomfort level above 9 (on 20-point Borg's scale), and all would work at a discomfort level of 2. Oh et al. (1997) studied the relationship between isometric and eccentric strength (EMG) against different tool velocities for varying torques and orientations. The results found that the handle was most stable (average velocity) when torque was 25 Nm, vertical was closest, and horizontal was farthest. Greater handle stability

was observed for horizontal workstations than for vertical, and hard joints resulted in 307% greater peak velocity than soft joints. This was confirmed with EMG, where the average latency was 38 ms for hard joints and 171 ms for soft joints.

Lin et al. (2007a) compared EMG activity of forearm flexors, extensors, and biceps with operator experience. Average EMG scaled to reference values (RVC) were greater for experienced users (318%, 285%, 143% RVC respectively) than for novice users (246%, 219%, 113% RVC respectively), as shown in Figure 2.9. This suggested that experienced users exerted more reaction force when using right-angle tools. This was validated with experienced users allowing only 7.9° handle displacement, compared to 11.5° for novice users. Similarly, Lin et al. (2010a) compared muscle activity for fastening and unfastening cycles, previously neglected in literature, and found that EMG activity in trapezius muscles was higher for unfastening cycles, further suggesting a potential risk for injury. Forsman et al. (2002) tested EMG activity in five muscles and found large variance in both within and between subjects, providing further insight on task parameters that cause least exertion. Steingraber et al. (2021) showed that a rapid, short duration tightening strategy (TurboTight) produces lower EMG magnitudes than conventional longer duration strategies, which also resulted in lower handle forces and displacement.

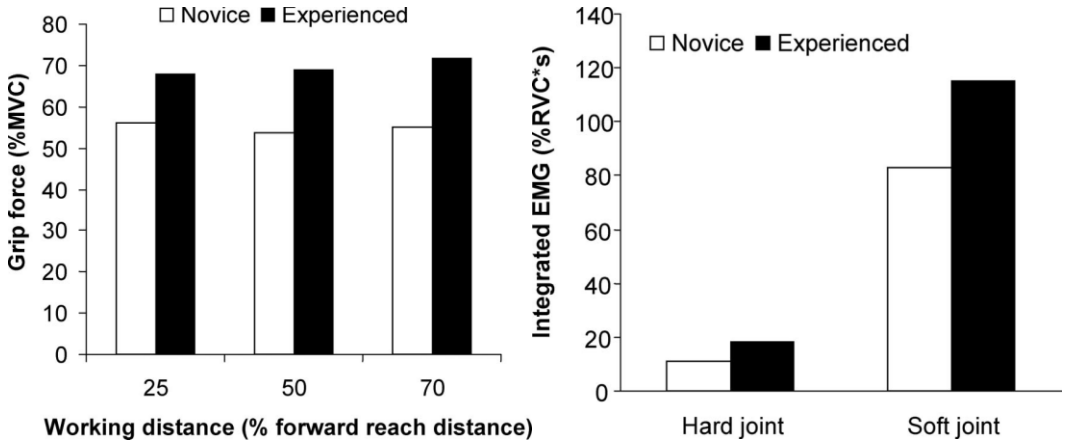

Figure 2.9: Comparison of EMG and grip force for operator experience levels (Lin et al., 2007a)

Lin et al. (2010b) with near-infrared spectroscopy (NIRS) observed that the deoxygenation levels were greater for flexor muscles than for extensor muscles, suggesting a greater metabolic demand from flexors during tool tightening. Conversely, tissue oxygenation index for extensors were greater in fast-paced, no rest tasks, suggesting fast-paced operations resulted in decreased oxygen saturation. Similarly, Lin et al. (2012) showed that average gripping force (as % MVE) was higher for fast-paced, no-rest tasks. Subjective Borg's ratings also reflected greater discomfort for such tasks. McGorry et al. (2009) evaluated muscle oxygenation and blood volume during gripping tasks for various handle diameters. The results showed that the average hemoglobin saturation, cHb, and total hemoglobin were significantly different in 30- and 40-

mm handles than with 50 mm. This suggested that smaller handles had similar oxygenation demands, whereas less hemoglobin was available for gripping larger handles. Sesto et al. (2005) used MRI to assess edema and found the average isometric strength decreased 42% immediately after tool operation and pain persisted for 2 days. The study also showed that exercised arms had a 360% increase in supinator-extensor relaxation time (a measure of edema), whereas non-exercised arms showed no difference. Self-reported pain levels were reported, with an average level of 4.1 (on 10) and remained at 1.97 two days after the experiment. This indicated a relation potential relationship between task parameters, physical demands, and recovery time.

Chang et al. (1999) tested different gloves and wrist supports for in-line pneumatic tools. Results indicated that wearing a nylon glove and not using a wrist support was the best combination for the tested conditions. Wearing a nylon glove reduced the triggering finger force by 18.2% when compared to bare hands, and EMG indicated that nylon glove had relatively lower forearm muscular exertion. However, the thickness of gloves had a negative effect, suggesting the use of optimal thickness gloves. Further, results also showed wrist supports required a greater triggering finger force, and such supports are appropriate only for protecting an injured wrist or strained area. However, it is not recommended for regular tightening tasks. Chang et al. (2000) showed that hand-arm stress indicated by EMG was greater for far than middle and near work distances for in-line electric tools. Results also showed that the small finger had the greatest force contribution (30%), and index finger had the least contribution (19%).

2.4.3 Experimental Models

Description

Although analytical models provide a simplified method of assessing hand tool injures, it only allows for measurement of the effects of certain parameters that were part of the model. An important consideration of modern power hand tools is that the tool controller allows a great deal of flexibility in setting tightening parameters and torque input profiles. For example, the tool speed, torque build-up time, rotation limits of fasteners, and different tightening strategies can all be set at the tool controller. These factors have a significant impact of the dynamic interaction between tool and operator, and therefore it is important to quantify the ergonomic impact of these settings, However, it is difficult to include it in a mathematical model. These parameters can only be investigated experimentally using test rigs and tool simulators.

Ay et al. (2017) developed a test rig that provided a means to simulate the dynamic response of the hand while operating a right-angle tool. The rig accounts for the variation in model parameters (stiffness, damping, mass) that correspond to each operator with respect to the working conditions such as joint hardness and target torques. The rig also allows for evaluating different right-angle tools, providing a

greater flexibility. Ay et al. (2010) describes the design and development of this test rig and is shown in Figure 2.10.

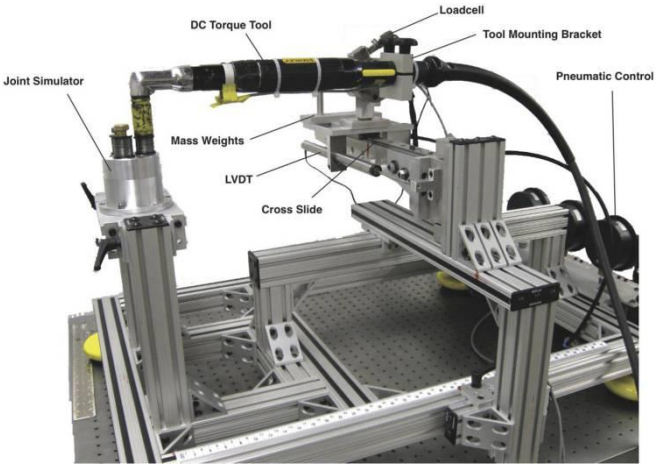

Figure 2.10: Test rig (or simulator) for a right-angle tool (Ay et al., 2017)

Lin et al. (2006) demonstrated a method of direct measurement of force at the interface between the tool handle and operator. A full factorial experiment was used to evaluate the effects of work distance, tool type, and joint hardness on the handle displacement and grip forces. Each tool consisted of a simulated handle with a stainless-steel core and instrumented with strain gauges that directly measure the grip forces and reaction moments. Lin et al. (2007b) used the same setup to provide additional data relevant to exposure assessment and suggested some enhancements to ISO 6544, which standardized a test method for measurement of reaction torque and torque impulse.

Results

Ku et al. (2007) investigated the relationship between tool properties (geometry, inertial properties, motor characteristics), fastener properties, orientation, and operator position for 69 workstations using 15 different pneumatic nutrunners. The study found that the tool shape and joint hardness both affected the handle forces and displacements ($p<0.05$). It was observed that the peak handle force and displacement for right-angle tools were twice greater than pistol grip tools. Meanwhile, soft joints had the greatest reactions. This was further validated by Lin et al. (2007b), where a simulated handle was used to demonstrate that soft joints produced greater reaction impulses than hard joints.

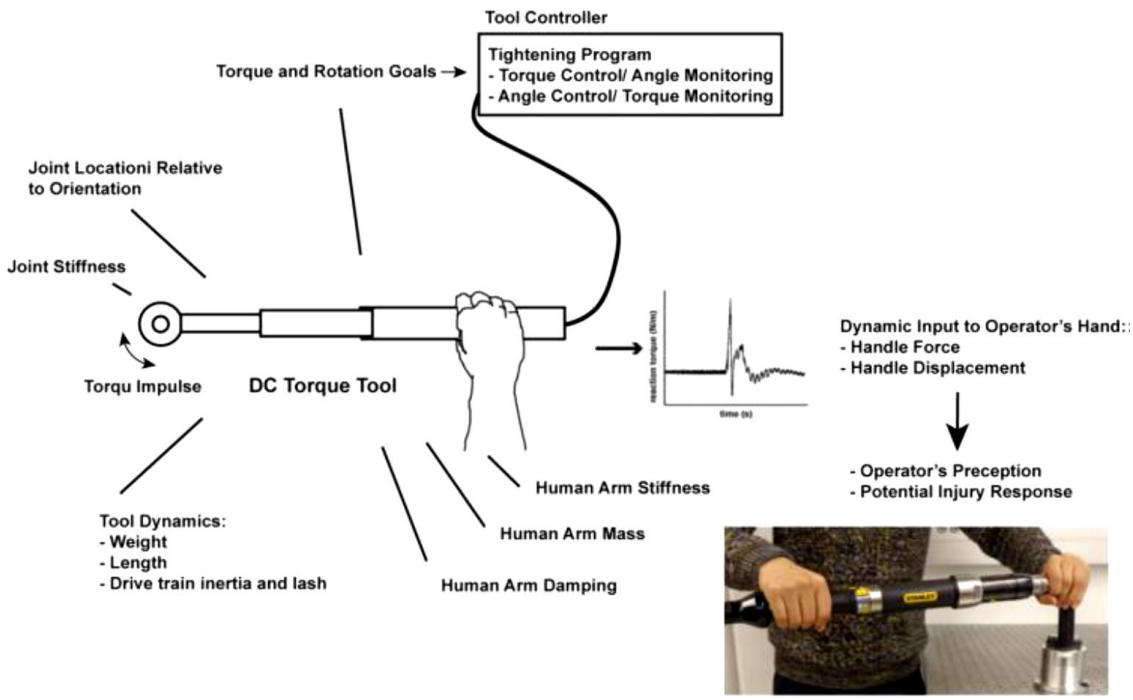

Figure 2.11: Tool dynamics simulation parameters (Ay et. al, 2017)

Ay et al. (2017) measured the tool handle force and displacements from the simulating test rig for different right-angle tools. The results found that the coefficient of determination between the test rig and human testing measurements were 0.98 and 0.85 for peak force and displacement respectively. Figure 2.11 describes the tool simulation parameters involved during operating the test rig.

2.4.4 Summary

Overall, the studies presented in this scoping review provided meaningful insight into the operator response mechanisms during power hand tool tightening operations. However, like most studies, several gaps and limitations were identified. The most obvious limitation was the presence of several task-related variables that influence the operator response behaviour. Although the studies mentioned here tried to model multiple variables, there was no single study that tested the influence of every parameter simultaneously. Consequently, a standardized methodology to test the phenomenon is currently unavailable for pistol grip tools. Although pneumatic power hand tools have some established standards for measurement of torque and reaction parameters, no standards for testing electric hand tools were found. Most research has been largely emphasized on pneumatic tools. As electric tools are becoming increasingly popular in industries, more research needs to be dedicated towards them.

Analytical models provide a simplified method to test reaction parameters. Models presented in this study assume a single degree-of-freedom linear nature. However, actual tool operation is non-linear, and

displacements could occur in higher degrees-of-freedom, and future studies should consider modelling non-linear parameters. While some non-linear models exist, it is known that the linearity assumption is valid if the operation is less than 500 ms (Lin et al. 2001; Ay et al., 2017). However, that presents another issue of very few studies considering the duration of exposure. Soft joints could potentially expose the operator to reaction loads longer than 500 ms, and further research is required to explore these effects. Further, the model developed by Lin et al. (2001) considered the inertial properties of the operator hand and tool body. The model failed to consider the inertial properties of other components such as cables, pneumatic pipes, and attached sensors that could potentially be influencing factors to the reaction specifically during rotational dynamics. Lin et al. (2003b) randomized trial orders and included rest breaks for the experiment; however, no subjective reports were available to prove fatigue was avoided. In studies testing for gender-based differences, the sample sizes of male and female were significantly different and hence could account for statistical errors. Some studies recruited only inexperienced operators, which is likely to underestimate operator capacities.

Physiological changes primarily responsible for aggravation of musculoskeletal injuries was not clear. Surface EMG was commonly used to measure muscle activity. However, it can only be used for superficial muscles; influence of other groups could not be explored. No standard electrode placement method was observed, and different studies measured different muscle groups ranging from forearm to the spine (which has no significant influence). Further, EMG values could be affected by movement and noise from the subject, and hence inconsistent response patterns were observed (Kihlberg et al., 1993). Lin et al. (2010a) conducted paired t-tests on joint hardness but revealed no information on the effects of other working condition variables that might affect the size of difference between fastening and unfastening cycles. Further research is required to explore the relation between unfastening cycles and risk of injury. Lin et al. (2010b) only performed linear regressions, so the analysis could not capture any non-linear variance within a session. Other limitations could be associated to the subjective ratings of operators, which do not necessarily reflect objective physiological changes. A more comprehensive correlation between subjective responses and physiological changes is required.

The test rig developed by Ay et al. (2017) had some limitations as well. The rig underestimated the operator responses slightly due to the inherent stiction in the cylinder used to represent arm stiffness. Another reason could be due to the assumption that the inherent damping from friction and air cylinder damping was sufficient to model the arm damping. No separate dampers were used; future test rigs could include separate dampers such as electrorheological (ERF) dampers. Also, the test rig only included right-angle tools; future rigs could be developed for pistol grip and in-line tools as well. Further, more comprehensive acceptability

limits, workplace ergonomics suggestions and tool design recommendations are required for tool operators and tool manufacturers.

2.5 Hypothesis

The current study addresses the gaps and limitations of previous research work identified in Section 2.4. In this study, a DC-cable-powered, pistol grip tool was considered to develop the analytical model, an experimental simulator, and further conduct a parametric study to test effects of various fastening parameters. Based on this approach, it is hypothesized that:

1. The analytical model will extract the operator parameters, and values will be within the range of typical hand-arm muscle forces.
2. The pistol grip tool simulator will emulate the handle displacement reaction of a typical tool operation with reasonable accuracy.
3. The parametric study on fastening parameters will reveal their optimum conditions that would effectively result in minimized handle displacements.

Chapter 3

Methodology

This methodology consists of four sections, each representing the objectives outlined in Chapter 1. Section 3.1 presents the analytical used to represent the human hand-arm and pistol grip tool multibody system. Each of the system parameters were identified and measured experimentally. Section 3.2 includes the in-vivo study conducted on tool operators to estimate their characteristics that influence tool reaction dynamics. Section 3.3 presents the design and development of a pistol grip tool simulator that emulates the dynamics of a typical fastening operation. Finally, Section 3.4 presents the experiments performed on the tool simulator to test the effects of various system parameters on the displacement of the tool handle.

3.1 Analytical Modelling

3.1.1 System and Parameter Identification

The aim of identifying the system was to determine the parameters required to model the dynamic interaction between the torque tool and the human operator, and further design a tool dynamic simulator. A deterministic approach was considered in identifying the parameters involved in representing the system. The system parameters are broadly classified into three categories, namely tool variables, task variables, and operator variables.

Tool Variables

Figure 3.1: Pistol grip tool

The toque tool considered was an Atlas Copco – Model ETP ST32-10-I06 – pistol grip electric nutrunner, as shown in Figure 3.1. The tool variables considered were the tool shape, tool weight, mass moment of inertia, location of centre of gravity, length of tool handle, and control algorithm of tightening algorithm. Although the tool control algorithm is highly configurable, only the torque and speed controls were considered in the model.

Task Variables

The selection criteria for task variables essentially depended on the type of fasteners and the threaded component they were being fastened to. The task variables were identified as the fastener tightening torque, joint stiffness, orientation of the tool relative to the operator, and the vertical and horizontal distance of the fastener relative to the operator.

Operator Variables

The operator variables considered were the width of the palm along the tool handle, location of individual metacarpophalangeal joints relative to the tool handle, hand-arm weight, overall body posture of the operator, strength or ability to resist the reaction torque, forearm muscle forces (EMG), expertise in using the tool, and general health of operator.

3.1.2 Modelling hand-arm dynamics

It was identified that all parameters outlined in Section 3.1.1 are involved in influencing the tool handle displacement, and hence considered in developing the analytical model. A model similar to the one presented by Lin et. al. (2001) was used in this study. Considering the dynamic behaviour of pistol grip tool operation, the hand-tool system was simplified into a single degree-of-freedom torsional model. The model represents the human operator as a subsystem consisting of a linear spring, a viscous damper, and a mass element. In reality, several muscles and joints contribute individually to performing a tightening task. However, the current model combines the loading of all involved muscles and joints into lumped mechanical elements without considering the direction of the loads. The lumped mechanical properties were assumed to be passive and constant for an operator at a given body posture and tool orientation. The effective spring stiffness and damping represent the total effect of resistance exerted by the operator against the tool handle. This includes contributions from the entire body. Therefore, the elastic and damping parameters of the model are unique to each operator and the given task. Similarly, the effective mass represents the total mass of the tool and the operator's hand-arm acting against the reaction torque. A pictorial representation of the single degree-of-freedom torsional model is shown in Figure 3.2.

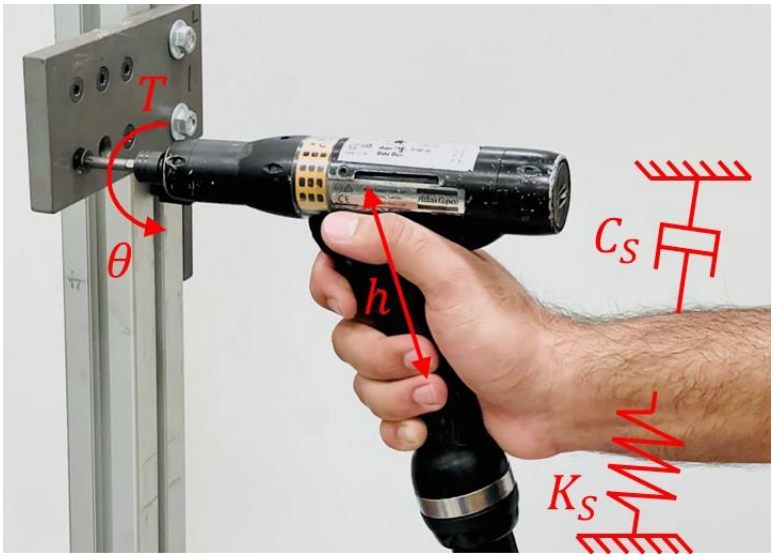

Figure 3.2: Single degree-of-freedom torsional model

Forward Dynamics

For any given spring (K), mass (M), and damper (C) system with an externally applied force, F, the equation of motion (x) can be expressed as a second order differential equation, as shown in Equation 3.1.

$$M\frac{d^2x}{dt^2} + C\frac{dx}{dt} + Kx = F(t) \qquad \text{Eqn. (3.1)}$$

Equation 3.1 can be further rewritten by converting force, F to torque, T acting at radius, h from the axis of rotation. Therefore, a torsional, dynamic equilibrium equation was derived about the tool spindle axis. The differential equation in terms of the tool handle rotation, θ is written as shown in Equation 3.2.

$$I_{ts}\frac{d^2\theta}{dt^2} + C_s h^2\frac{d\theta}{dt} + K_s h^2\theta = T(t) \qquad \text{Eqn. (3.2)}$$

Where,

$T(t)$ = Tool reaction torque, with respect to time (Nm)

K_s = Effective stiffness of the operator (N/m)

C_s = Effective damping of the operator (Ns/m)

h = Location of resistance exerted by the operator from the spindle axis (m)

θ = Angular displacement of the tool handle (rad)

$I_{ts} = I_{tool} + I_{subject}$

I_{tool} = Mass moment of inertia of the tool (kgm^2)

$I_{subject}$ = Mass moment of inertia of the operator hand (kgm^2)

The mass moments of inertia, I_{ts} is the total mass moment of inertia of the system which includes, the mass moment of inertia of the tool, and mass moment of inertia of the operator hand-arm. The reaction torque which is a result of the response due to tightening is represented by T, varying with respect to time, t. The effective stiffness of the operator exerting resistance against the reaction torque is represented by K_s. Similarly, the effective damping of the operator due to reaction resistance is represented by C_s. The resistance exerted by the operator hand was assumed to be concentrated at a single point along the tool handle. The distance from this point of load application on the tool handle to the tool spindle axis is represented by h. The angular displacement of the tool handle with respect to the tool spindle axis is represented as θ. Further, the angular velocity and angular acceleration of the tool handle was derived by differentiating θ with respect to time, t. Since the angular displacement varies with respect to each time step, Δt, the angular velocity, $\dot{\theta}$ and angular acceleration, $\ddot{\theta}$ were derived using three-point differentiation method and are shown in Equation 3.3 to Equation 3.6.

$$\dot{\theta}_n = \frac{\theta_{n+1} - \theta_{n-1}}{2\,\Delta t} \qquad \text{Eqn. (3.3)}$$

$$\ddot{\theta}_n = \frac{\dot{\theta}_{n+1} - \ddot{\theta}_{n-1}}{2\,\Delta t} = \frac{\theta_{n+1} - 2\,\theta + \theta_{n-1}}{\Delta t^2} \qquad \text{Eqn. (3.4)}$$

Where,

$$\dot{\theta}_{n+1} = \frac{\theta_{n+2} - \theta_n}{2\,\Delta t} \qquad \text{Eqn. (3.5)}$$

$$\theta_n = 2\,\Delta t\left(\dot{\theta}_{n-1}\right) + \theta_{n-2} \qquad \text{Eqn. (3.6)}$$

n = increments from 1 to total number of time steps

Finally, the effect due to gravity was not considered in Equation 3.2 since the orientation of the system varies depending on the direction of the fasteners; for example, as shown in Figure 2.8.

Inverse Dynamics

In Equation 3.2, the distance of hand force application, h, mass moment of inertia, I_{ts}, torque, T, and angular displacement, θ are system intrinsic properties and were measured through experiments. Whereas the operator parameters, namely effective stiffness, effective damping, and hand mass moment of inertia are operator intrinsic properties. The stiffness and damping were predicted using an inverse dynamics approach. These identification parameters are set up in time domain with torque, T as the input and angular displacement, θ as the output. The inverse dynamic equation is expressed as shown in Equation 3.7.

$$[T - I_{ts}\ddot{\theta}]_{n\times 1} = \begin{bmatrix} \theta_1 & \dot{\theta}_1 \\ \cdot & \cdot \\ \cdot & \cdot \\ \theta_n & \dot{\theta}_n \end{bmatrix}_{n\times 2} \begin{bmatrix} K_s h^2 \\ C_s h^2 \end{bmatrix} \qquad \text{Eqn. (3.7)}$$

Equation 3.7 produces an overdetermined system of *n* equations and 2 unknowns. The number of equations, *n* is equal to the number of samples collected during the torque build-up period i.e., the sampling frequency of measuring the torque and angular displacement. Since the duration of torque build-up varies with each trial, the number of equations also vary correspondingly. The damping parameter, C_s was assumed to be negligible and was neglected for further calculations (Lin et. al., 2003c). Using the above time domain setup with *n* equations, the single unknown stiffness parameter, K_s was calculated by isolating the variable. This produces a unique stiffness value at each time step. This parameter represents the elastic characteristics of each operator during torque build-up period. Equation 3.7 was evaluated using Matlab code, as outlined in Appendix A.

3.1.3 Mass moment of inertia calculation

Experiments were conducted to measure each parameter in the analytical model of the tool-operator system. The mass moment of inertia of the system about the spindle axis was determined to be a summation of the individual mass moments of inertia of the tool and operator hand-arm. However, the pistol grip tool consists of the tool body and the tool cable attached to the handle. Owing to the irregular mass distribution and location of centre of mass of the pistol grip tool, the mass moments of inertia of the tool body and tool cable were measured individually. The mass moment of inertia of the tool body was measured using two oscillation methods – bifilar pendulum method and simple pendulum method.

Bifilar Pendulum Method

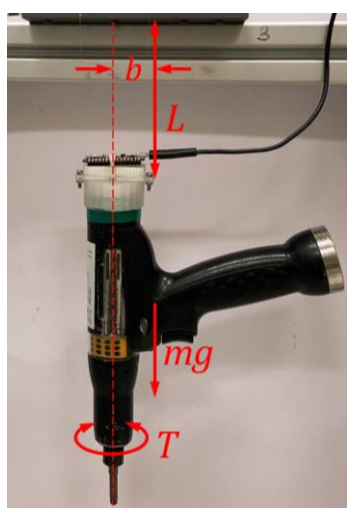

Figure 3.3: Bifilar pendulum experimental setup

The bifilar pendulum experiment consisted of suspending the tool body as shown in Figure 3.3. The tool was suspended vertically using two nylon cables of negligible mass and equal length L, placed equally apart by b from the axis of rotation of the tool spindle. The mass of the tool is given by m, the time period for each oscillation is given by T, and g is the acceleration due to gravity. The time period of oscillation was measured using a LSM6DSL 6-Axis IMU (Inertial Measurement Unit). A small perturbation was given to the tool such that the resulting free oscillation was pure rotation about the spindle axis. The oscillations were recorded for 12 trials, as shown in Figure 3.4.

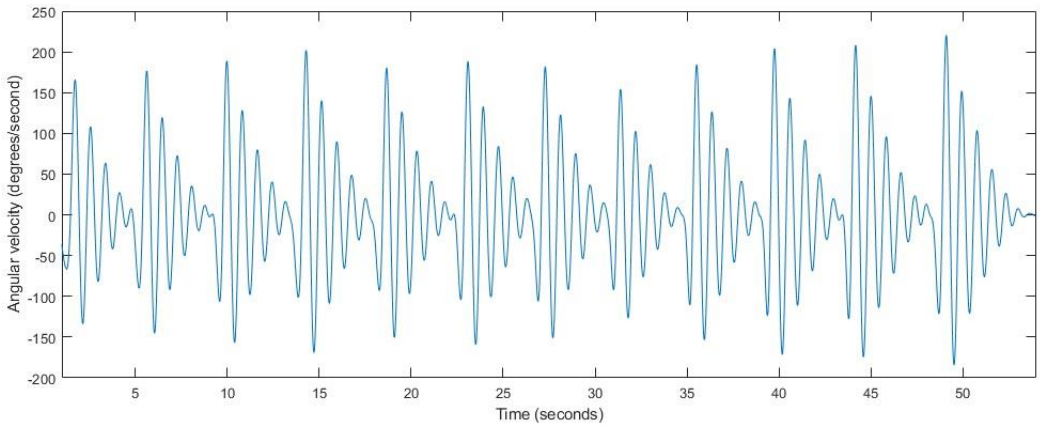

Figure 3.4: Angular velocity of tool body from bifilar pendulum experiment

The time period of the initial three oscillations during all 12 trials were considered in calculating the mass moment of inertia and are tabulated in Table 3.1.

Table 3.1: Time period of oscillations of bifilar pendulum experiment

Trial No.	Time period of oscillation, T (s)			Mean time period (s)
	1st cycle	2nd cycle	3rd cycle	
1	0.8881	0.8232	0.7857	0.8323
2	0.8707	0.8274	0.7984	0.8322
3	0.8599	0.8324	0.8036	0.8320
4	0.8786	0.8359	0.8096	0.8414
5	0.8574	0.8205	0.7990	0.8256
6	0.8548	0.8247	0.7968	0.8254
7	0.8510	0.8286	0.7924	0.8240
8	0.8398	0.8163	0.7821	0.8127
9	0.8462	0.8233	0.7946	0.8214
10	0.8550	0.8293	0.8029	0.8291

11	0.8548	0.8325	0.8071	0.8315
12	0.8669	0.8359	0.8113	0.8380
Mean	0.8603	0.8275	0.7986	0.8288

Further, the mass of the tool body, suspension cable length, inter-cable width and mean time period of oscillation are given in Table 3.2.

Table 3.2: Bifilar pendulum experimental setup

m (kg)	L (m)	b (m)	T (s)
0.824	0.05745	0.02277	0.8288

Therefore, the mass moment of inertia of the tool body was calculated as shown in Equation 3.8.

$$I_{body-bifilar} = \frac{mgb^2T^2}{4\pi^2L} = 0.00127\ kgm^2 \qquad \text{Eqn. (3.8)}$$

Simple Pendulum Method – Validation

Although the bifilar pendulum experiment offered a reasonable approximation of the mass moment of inertia of the tool body, this value was further validated using a simple pendulum experiment. In this method, the tool body was assumed to be a simple pendulum whose mass is concentrated at the centre of mass (COM) of the tool body. The centre of mass of the tool body was identified by suspending the tool by a single nylon in three different axes individually. The point of intersection of the three axes was assumed to be the centre of mass. By taking advantage of the cylindrical shape of the tool head, it was allowed to freely oscillate over a horizontal surface, as shown in Figure 3.5. The surface was secured to be flat and horizontal using an IMU mounted onto a linear bearing that slides over the two T-slotted extrusions.

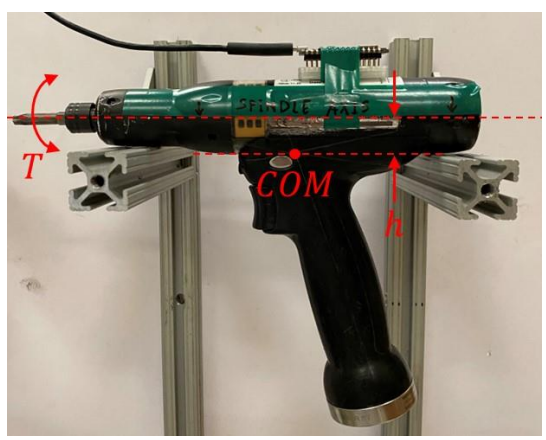

Figure 3.5: Simple pendulum experimental setup

The distance between the centre of mass and the tool spindle axis is expressed as h, and was measured to be 0.018 m. A small perturbation was applied such that the tool rotated about the spindle axis over the surface, without any slipping or sliding. The oscillations were recorded with a LSM6DSL 6-Axis IMU for 6 trials, as shown in Figure 3.6.

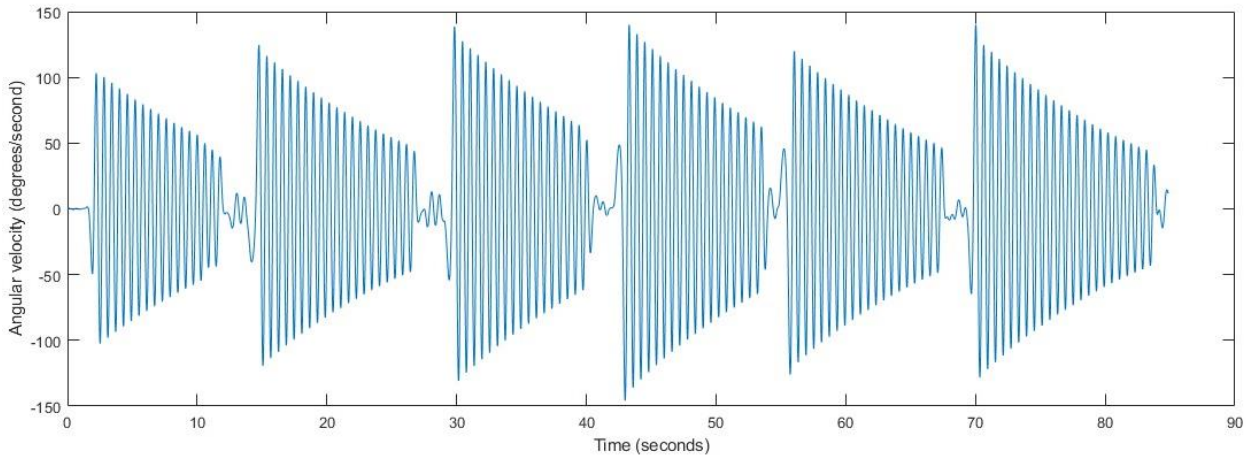

Figure 3.6: Angular velocity of tool body from simple pendulum experiment

The mean time period of oscillation, T of each cycle was found to be 0.6 seconds; or the frequency of oscillation, f was 1.6667 Hz. Therefore, the mass moment of inertia of the tool body using simple pendulum method was derived and calculated as shown in Equation 3.9.

$$I_{body-pendulum} = \frac{mgh}{(2\pi f)^2} = 0.001327\ kgm^2 \qquad \text{Eqn. (3.9)}$$

It was observed that the mass moments of inertia from bifilar and simple pendulum methods provided a reasonable estimation. Therefore, the average value derived from both methods was approximated for further considerations, as shown in Equation 3.10 and 3.11.

$$I_{body} = \left(I_{body-bifilar} + I_{body-pendulum}\right)/2 \qquad \text{Eqn. (3.10)}$$

$$I_{body} = 0.0013\ kgm^2 \qquad \text{Eqn. (3.11)}$$

Tool Cable

Further, the mass moment of inertia of the tool cable was estimated. Owing to the complex lengthy geometry of the tool cable, no reasonable experimental method was found to provide a reasonable estimation. Alternatively, the tool cable was assumed to be a lumped mass at the free end of the tool handle, representing a simple pendulum. While tool operators use the tool at various locations relative to the ground (Low, High, Under, Right, as outlined in Section 3.2.2), it was assumed that the weight of the cable varied

corresponding to each fastener location. The end of the cable was suspended freely, and the weights were measured using a Tektronix Mark-10 digital force gauge. The weights of the cable at each location are shown in Table 3.3.

Table 3.3: Cable weight at four fastener locations

Fastener Location	Cable Weight (kg)
Low	0.4077
High	0.5504
Under	0.5198
Right	0.3975
Mean, m_{cable}	0.4688

The mean weight of the tool cable, m_{cable} was considered for further calculations. The distance between the free end of the tool handle and the tool spindle axis, l_{handle} was measured to be 0.138 m. Therefore, with a simple pendulum assumption, the mass moment of inertia of the tool cable was calculated as shown in Equation 3.12.

$$I_{cable} = m_{cable}\left({l_{handle}}^2\right) = 0.008928\ kgm^2 \qquad \text{Eqn. (3.12)}$$

Therefore, the total moment of inertia of the tool along with the cable was calculated as a summation of the tool body and the tool cable, as shown in Equation 3.13.

$$I_{tool} = I_{body} + I_{cable} = 0.01023\ kgm^2 \qquad \text{Eqn. (3.13)}$$

Operator Hand-Arm

The mass moment of inertia of the operator hand-arm was also estimated similarly using a simple pendulum assumption. The hand-arm was assumed to be a lumped mass acting as certain distance from the spindle axis on the tool handle. The mass of a human hand-arm, m_{hand} was derived as a proportion of the total human body weight, m_{body}, as outlined in the Dempster's table (Winter, 2009). The mass of the hand-arm is given by Equation 3.14.

$$m_{hand} = 0.006(m_{body}) \qquad \text{Eqn. (3.14)}$$

Further, the location of the lumped hand-arm mass was assumed to be the centre of pressure of the mean grip force exerted on the tool handle. Previous studies conducted by Loewen (2019), estimated the centre of pressure of grip force on the tool handle. It was observed that the centre of pressure corresponded to the location of the 4th metacarpophalangeal joint, or commonly referred to as the ring finger knuckle. The

variation of this location between operators was assumed to be negligible and was not considered in the calculations for mass moments of inertia. However, the distance between the spindle axis and location of the centre of pressure, l_{COP} was approximated to be 0.09 m. Therefore, the mass moment of inertia of the operator hand-arm was derived and calculated as shown in Equation 3.16.

$$I_{subject} = 0.006(m_{body})({l_{COP}}^2) \quad \text{Eqn. (3.15)}$$

$$I_{subject} = 0.0000486(m_{body})\ kgm^2 \quad \text{Eqn. (3.16)}$$

Total Mass Moment of Inertia

The individual mass moments of inertia of each component that had a significant influence on the tool reaction dynamics were estimated. Therefore, the total moment of inertia of the tool and operator system was calculated as a summation of the individual components, as shown in Equation 3.17.

$$I_{ts} = I_{tool} + I_{subject} \quad \text{Eqn. (3.17)}$$

$$I_{ts} = [0.01023 + 0.0000486(m_{body})]\ kgm^2 \quad \text{Eqn. (3.18)}$$

Where, m_{body} is the total body weight of the tool operator in kg. Corresponding to each operator, the individual mass moments of inertia were used in the inverse dynamic equation to predict the effective stiffness parameter.

3.2 In-Vivo Study

Followed by the measurement of mass moment of inertia of the system, the remaining parameters in the analytical model were estimated by conducting in-vivo experiments on tool operators.

3.2.1 Participants

The study was approved by University of Waterloo's Office of Research Ethics and conducted at the manufacturing plant of the industrial partner, Honda of Canada Manufacturing (HCM) situated in Alliston, Ontario. Fifteen workers voluntarily participated in the study. All participants were informed of the experimental procedure, equipment used, data collected, and potential risks involved in performing the tasks. Participants were also informed that if at any point during the study they wish to stop for any reason, they could do so. Finally, a written consent was received from each participant agreeing to participate in the study. Of the fifteen participants, five participants were excluded as outliers in this study due to technical errors during experiments, and failure to complete tasks reasonably. Therefore, only ten participants were considered as feasible for the analysis of this study. All ten participants reported to have used a pistol grip tool in the assembly line at some point during their time at HCM and were considered as experienced tool

operators. No pre-existing injuries or fatigue were reported prior to the study. Of the ten participants, eight participants were male, and two were female. All participants were right-handed tool operators. The anthropometrics of all participants are listed in Table 3.4.

Table 3.4: Anthropometrics of participants from in-vivo study

Participant	Sex (M/F)	Age (yrs)	Weight (kg)	Height (cm)	Elbow Height (cm)	3rd MCP (cm)
S1	F	21	57.5	166.4	106.7	2.5
S2	M	21	74.2	186.4	113.0	3.3
S3	M	53	61.5	169.7	138.4	3.4
S4	M	56	88.8	170.2	134.6	3.5
S5	M	36	92.5	183.9	151.9	3.4
S6	M	57	93.9	188.0	152.4	3.6
S7	M	27	133.2	179.3	142.7	3.3
S8	M	43	107.1	175.3	144.8	3.4
S9	F	32	59.2	168.1	137.9	3.0
S10	M	42	72.0	171.2	136.4	3.4
Mean	N/A	38.8	84.0	175.9	135.9	3.3
SD	N/A	13.7	24.1	8.0	15.1	0.3

In Table 3.4, 3rd MCP refers to the distance from the centre of the 3rd metacarpophalangeal joint (middle finger knuckle) to the radial end of the palm, neglecting the thumb. This was used as a measure of hand span to observe for any significant variations. The elbow height was considered as a measure of the neutral position at which the operator holds the tool during 90° elbow flexion. Although these parameters were not directly used in modelling the operators, they were considered while identifying outliers among the participants.

3.2.2 Equipment

The tasks in this study primarily involved fastening screws into a threaded plate using the Atlas Copco pistol grip tool. Technical specifications of the tool are given in Table 3.5.

Table 3.5: Technical specifications of pistol grip tool

Parameter	Value
Model	ETP ST32-10-I06
Shape	Pistol grip
Max speed	1210 RPM
Torque range	3–11 Nm
Drive size	¼ in.
Length	197 mm
Height	179 mm
Weight	0.825 kg
Motor power	1400 W
Motor Voltage	200 V, 3 a.c.

The tool was connected to an Atlas Copco Power Focus controller which was used to program the tool operation. The controller was programmed using the Toolstalk PF designated software package, shown in Figure 3.7. The torque about the spindle axis was measured using the tool's built-in torque sensor. The angular displacement of the tool handle was measured using the tool's built-in rotary variable differential transformer (RVDT).

Power Focus controller

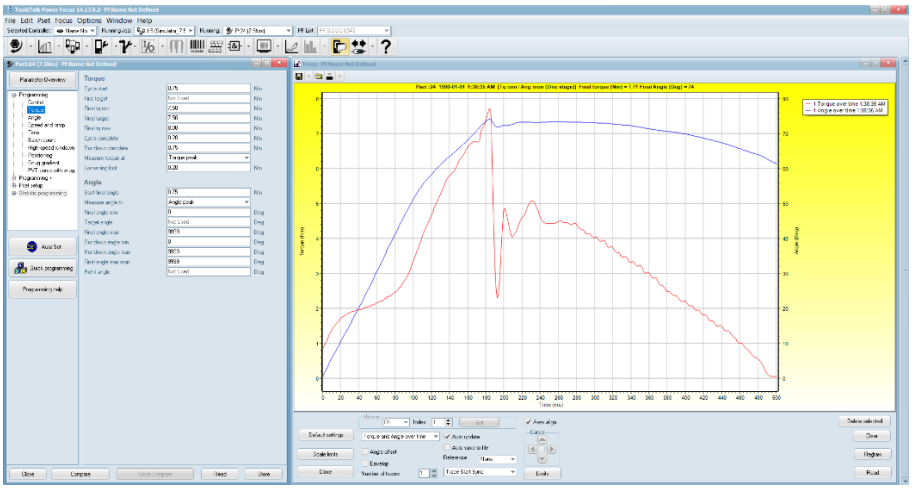

Toolstalk PF software

Figure 3.7: Tool controller and software interface

Further, HCM reported the routine use of flat headed fasteners in their assembly line. The fasteners used in this study are M6 × 1 mm – 16 mm long, flat head, Torx plus drive, alloy steel screws. A T30 Torx Plus Steel drive bit was used to fasten the screws. A test frame was built with aluminum T-slotted extrusions and mounted onto a table. Four steel plates with M6 × 1 mm threaded holes, and 90° countersink angles were attached at four different locations on the test frame, as shown in Figure 3.8.

Figure 3.8: Fastener locations used during in-vivo study

Each location corresponded to different orientations of the operator wrist. The 'Low' and 'High' locations corresponded to two degrees of ulnar deviation of the wrist, at heights of 130 cm and 180 cm from the ground respectively. The 'Under' location corresponded to radial deviation of the wrist at a height of 180 cm from the ground. The 'Right' location corresponded to wrist flexion at a height of 130 cm from the ground. These locations were typical at HCM and within reasonable reach for all participants.

3.2.3 Experimental Procedure

A standardized testing protocol was developed to collect data required to estimate the operator stiffness parameter. After the participant provided consent to participate in the study, the anthropometrics were recorded using conventional measurements. Later, the participants were allowed to use the tool for a few minutes to familiarize themselves with the tasks. Participants took a neutral, comfortable body position relative to the frame such that they were able to reach all fasteners, and the position was not altered during the experiments to maintain consistency in the results.

The protocol consisted of three sets, each corresponding to three different target torques at which the screws were to be fastened. HCM reported the typical range of torques used in the assembly line was 5 – 8 Nm. Therefore, the three torques considered in this study were 5 Nm, 7.5 Nm, and 10 Nm. The 10 Nm torque was considered to test the maximum limits of operator performance although it was not typical in the assembly line environment. Each set was performed in the order of increasing torques. Within each set consisted of four subsets corresponding to each location of the fastener on the test frame. Participants were asked to fasten three screws at each location, thereby performing three trials for each test condition. The locations were changed in the order of 'Low', 'High', 'Under', and 'Right'. A total of 36 screws were fastened by each operator (3 torques $\times$ 4 locations $\times$ 3 trials $=$ 36 screws fastened). The tool operating conditions are summarized in Table 3.6.

Table 3.6: Tool programming parameters

Condition	Description
Torque	5, 7.5, 10 Nm
Location	Low, High, Under, Right
Fastener	M6 $\times$ 1 mm, Flat Head
Spindle Speed	121 RPM
Control strategy	Torque control, Angle monitor
Tightening strategy	One stage
Sampling frequency	1000 Hz

Participants were provided with a 2-minute resting period between each set and were allowed to take a 1-minute break if they felt fatigued or if needed for any other reason. After the completion of all tightening tasks, participants answered a 3-minute questionnaire. The NASA Task Load Index (TLX) was used to assess the subjective workload experienced while performing the tasks. Table 3.7 summarises the six factors measured in the NASA TLX questionnaire.

Table 3.7: NASA Task Load Index (TLX)

Factor	Rating Scale (0 – 100)
Mental demand	Low – High
Physical demand	Low – High
Temporal demand	Low – High
Performance	Good – Poor
Effort	Low – High
Frustration Level	Low – High

Data Processing

As outlined in Section 3.2.2, the tool torque and angular displacement were directly from the in-built sensors within the tool. The Toolstalk PF software was used to record data for each trial. The angular displacement of the tool handle was measured relative to the rotation of the tool spindle, as the tool RVDT sensor only measured the spindle rotation. The angular displacement of was recorded from the start of the tightening phase i.e., when the tool torque reaches 10% of the target torque. Recordings were made until the fastener reaches the target torque, the tool motor automatically shuts-off, and the spindle rundown is complete. The default sampling frequency was 1000 Hz, so a data point for every 1 millisecond time step was recorded.

A Matlab code (Appendix A) was scripted to evaluate the inverse dynamic equation of motion of the single degree-of-freedom model outlined in Section 3.1. The torque and angular displacement data were extracted from Excel. A low-pass Butterworth filter with a cut-off frequency of 100 Hz was applied to the angular displacement data to filter high frequency noise. Further, ISO 5393 suggested the torque curve does not deviate from a straight line by more than 5% between 10% and 100% of the target torque. However, due to experimental conditions such as initial friction between the fastener and threaded joint plate, a higher threshold value was required. It was found that the experiments presented most usable data for all participants between 20% and 100% of the target torque during this study. Other model parameters were input into the script, and the effective stiffness of individual operators were evaluated for each of the 36 trials. The mean values of 3 trials for each condition was processed, as presented in Section 4.1.

It was observed that the effective stiffness values were not constant during the torque build-up time, which agreed with the non-linear, active, dynamic nature of human muscle exertions. However, for the current study, the values were assumed to be constant by considering the mean effective stiffness for the duration of the torque build-up (Figure 2.6). Therefore, a unique value of stiffness was approximated for each operator and experimental condition (torque and fastener location).

3.3 Design and Development of Tool Simulator

The in-vivo study in Section 3.2 presented a reasonable estimation of the operator specific parameters. However, due to ethical reasons, it was not feasible to test for other parameters within the system. The use of human operators for such tests puts the subjects under further risk of injury. Moreover, the parameters that are not studied cannot be controlled, for example grip force and angle of operation. Therefore, the goal of this part of the study was to design a mechanical simulator that emulates the dynamics of pistol grip tool operation by a human subject.

3.3.1 Functional Requirements

The functional requirements of the simulator were based on the need for a device to simulate the dynamic response of the tool handle during pistol grip tool operation, while incorporating the operator parameters. This included varying the effective stiffness corresponding to the desired task characteristics such as fastener location and operating torque. The rig also had to allow for the collection of accurate and repeatable reaction torque and angular displacement measurements simultaneously. The design is similar to the one developed for a right angle tool by Ay et. al. (2017), the main difference with this being able to simulate a pistol grip tool. The design was required to have a threaded joint plate to which screws would be fastened. The simulator also required a clamp that holds the tool handle to simulate a human hand holding it. To simulate the single degree-of-freedom rotational motion of the tool handle about the spindle axis, a kinematic mechanism was required to produce the same motion. Owing to the significant mass moment of inertia of the tool cable, the design demanded to accommodate its motion during tool response. Finally, the tool trigger needed to be actuated remotely and communicate with a connected computer. The design and kinematics of this simulator are discussed further in the following sections.

3.3.2 Kinematics of Mechanism

Two primary considerations were made in choosing a mechanism to simulate the reaction motion of the tool handle. First, the mechanism should produce the same single degree-of-freedom rotation about the spindle axis. Second, the mechanism should allow for an actuator to be attached such that it simulates the muscular effort of the human operator opposing the reaction torque. It was determined that a quick-return

mechanism would best satisfy these functional requirements and hence was chosen for the simulator design. A schematic representation of the quick-return mechanism is shown in Figure 3.9.

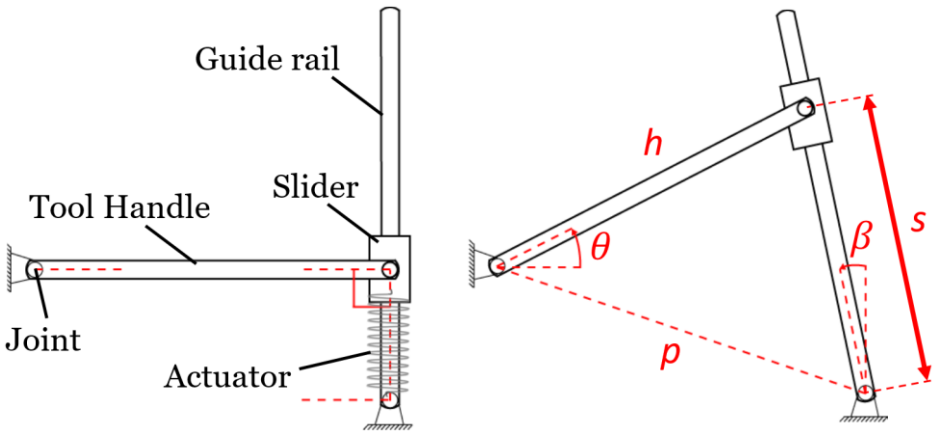

Figure 3.9: Quick-return mechanism of tool simulator (Ay, 2011)

It was noted that the mechanism consists of 3 revolute joints – tool joint, guide rail pivot, and slider-handle pivot. It also consists of 1 prismatic joint. Therefore, there are 3 bodies – 2 links, and 1 slider. This produced a single degree of freedom motion with the prescribed driver motion as the joint rotation about the spindle axis, denoted by θ. The joint represents the spindle axis which is orthogonal to the directions of the guide rail and tool handle. The length of the tool handle was denoted by h, which was incorporated as a variable in the kinematic model.

The mechanism was constructed upon the assumption that the tool was initially perpendicular to the linear guide rail. An actuator representing the operator parameters was placed along the direction of the guide rail. This allowed for the effective stiffness parameter to be acting orthogonal to the tool handle. The initial distance between the slider and guide rail pivot was denoted by s_0. At any time instance t, the guide rail rotation was denoted by β. The slider position on the guide rail was given by s. The distance between the spindle axis and guide rail pivot was denoted by p.

Therefore, an analytical kinematic model was developed to relate the angular displacement of the tool to the linear displacement of the slider along the guide rail. The geometric relationships were derived as shown in Equation 3.19.

$$p^2 = h^2 + {s_0}^2 = h^2 + s^2 - 2\,s\,h\sin(\theta - \beta) \qquad \text{Eqn. (3.19)}$$

$$\sin(\theta - \beta) = \frac{s^2 - {s_0}^2}{2\,s\,h} \qquad \text{Eqn. (3.20)}$$

The kinematic velocity equations are given by,

$$h\,\dot{\theta}\sin(\theta-\beta) = s\,\dot{\beta} \qquad \text{Eqn. (3.21)}$$

$$h\,\dot{\theta}\cos(\theta-\beta) = \dot{s} \qquad \text{Eqn. (3.22)}$$

$$\dot{\theta}^2 = \dot{s}^2 + s^2\dot{\beta}^2 \qquad \text{Eqn. (3.23)}$$

$$\dot{\beta} = \frac{s^2 - {s_0}^2}{2\,s^2}\dot{\theta} \qquad \text{Eqn. (3.24)}$$

Therefore, the angular velocity, $\dot{\theta}$ was expressed as a function of the slider velocity, $\dot{s}$.

$$\dot{\theta} = \left(\frac{1}{h}\right)\left[\frac{1}{1-\left(\frac{s^2 - {s_0}^2}{2\,s\,h}\right)^2}\right] \qquad \text{Eqn. (3.25)}$$

$$\theta(t) = \left(\frac{1}{h}\right)\int\left[\frac{1}{1-\left(\frac{s^2 - s_0^2}{2\,s\,h}\right)^2}\right]^{1/2} ds \qquad \text{Eqn. (3.26)}$$

Let f be a function of s,

$$f(s) = \left[\frac{1}{1-\left(\frac{s^2 - s_0^2}{2\,s\,h}\right)^2}\right]^{1/2} \qquad \text{Eqn. (3.27)}$$

Therefore,

$$\theta(t) = \frac{1}{h}\int f(s)\,ds \qquad \text{Eqn. (3.28)}$$

The above equation could be used to predict the angular displacement of the tool handle and validate the mechanism by comparing it with the measured angular displacement from the tool's RVDT.

3.3.3 Instrumentation and Design Elements

The structural frame of the simulator was primarily built using 1-inch and 2-inch-wide aluminum T-slotted extrusions. This allowed for great range of customizability and a modular design for the simulator.

Joint Plate

A similar steel joint plate from the in-vivo study was used to fasten screws. The threaded hole specifications were M6 × 1 mm, with a 90° countersink angle on one face, and flat surface on the other face. As observed in a typical fastening operation, the tool is required to move along the spindle axis as the screw is being fed

(or rundown) into the threaded hole. This linear displacement is essential to maintaining contact between the tool bit and screw head during the entire fastening period. Alternative to moving the tool, the joint plate was designed to move towards the tool using a slider and compression spring actuation. This allowed for building a more robust mechanism around the tool. The specifications of the spring were selected such that it provided just enough actuation to move the plate, maintain contact with tool bit, and to complete the fastening operation with reasonable accuracy. The design of the joint plate is shown in Figure 3.10.

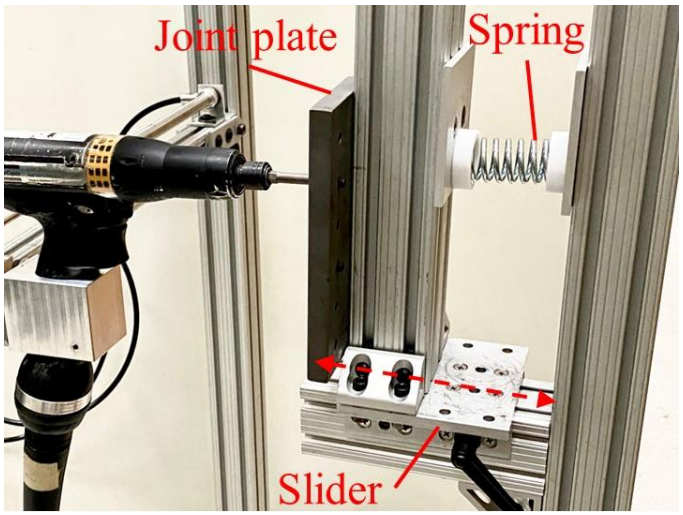

Figure 3.10: Joint plate design

Tool Holder and Slider

The holder was designed to clamp the tool such that it provided a unform distribution around the pistol grip contour of the tool handle. The holder was made of aluminum owing to its reasonable strength and light weight. The CAD model of the pistol grip handle was used to machine a cavity within the block using CNC, as shown in Figure 3.11.

Figure 3.11: Tool holder and sleeve bearing (dismantled)

Further, a custom tool slider was designed to translate over a 1-inch wide, square, T-slotted guide rail. The slider consisted of two linear bearing pads made of UHMW polyethylene to reduce friction while meeting the strength requirements. Due to the high bending loads experienced during tool operation, the slider was made of stainless steel to meet the design requirements. A 1/4 in. stainless steel rod was then welded to the tool slider. A revolute joint was created between the tool holder and the slider by mounting a flanged, dry-running, sleeve bearing on the tool holder, shown in Figure 3.11. It was ensured that the bearing axis of rotation was parallel to the spindle axis, as outlined in the kinematic model in Section 3.3.2.

Guide Rail and Actuator

The guide rail was a 1-inch wide, square, T-slotted extrusion made of aluminum. One end of the rail was pivoted to a fixed point on the structural frame of the simulator. The other free end of the rail was simply supported such that the rail was horizontal and parallel to the ground at its initial position. Further, due to the weight of the tool, holder, and slider acting on the guide rail, a counterweight was added by running a steel cable over a pulley. It was identified through trial and error that a counterweight of 10 N was sufficient to achieve a reasonable equilibrium of the guide rail pivot.

Figure 3.12: Pneumatic cylinder mounted on the guide rail

Besides the kinematic requirement, the guide rail was also used to mount the actuator chosen to represent the operator stiffness. After several considerations, the effective stiffness was simulated using a double-acting pneumatic air cylinder, as shown in Figure 3.12. The specifications of the air cylinder are summarized in Table 3.8.

Table 3.8: Technical specifications of air cylinder

Specification	Description
Actuation style	Double acting
Shape	Round body
Bore size	7/16”
Stroke length	8”
Rod diameter	0.19”
Actuation	Nitrogen
Inlet size	10-32 UNF
Material	Stainless steel

The air cylinder was mounted to the guide rail using custom brackets. The threaded end of the cylinder rod was mounted to the tool slider. The inlets were connected to a manual pneumatic control system. To account for the small difference in volumes, the pressure ratio of both plenums was found to be 0.8114. The pressure on both sides of the double acting cylinder was individually controlled using manual air regulators and digital pressure gauges mounted to the simulator control panel, as shown in Figure 3.13.

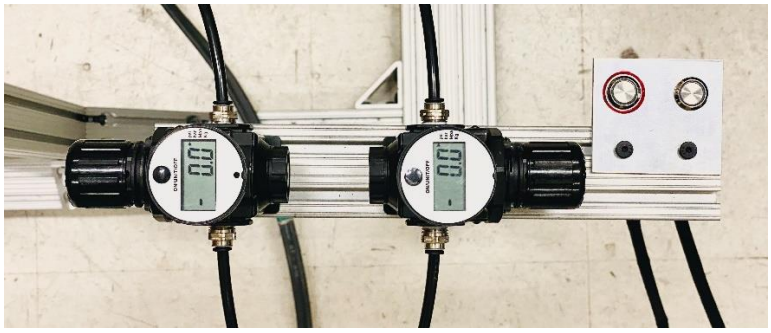

Figure 3.13: Simulator control panel

The control panel also comprised of two manual switches designed to remotely activate the tool trigger. Each switch corresponds to each direction of rotation of the tool spindle for tightening and loosening. The remote connection was achieved by using digital inputs to the Power Focus controller. Further, the effective damping of the tool operator was not instrumented and was assumed that the inherent damping of the simulator due to friction was sufficient. Finally, the pressure value corresponding to each effective stiffness value was to be derived and is summarized in Section 3.3.4.

3.3.4 Pneumatic Equivalent of Effective Stiffness

Using the pneumatic cylinder specifications, the effective stiffness was approximated as a linear function of the cylinder pressure. The cylinder rod was assumed to have an initial position at half the stroke length. It was assumed the system obeyed ideal gas law, with constant temperature, no leakage, and negligible friction.

V_{in} = Initial volume on each side of the cylinder (in^3)

P_{in} = Initial pressure on each side of the cylinder (psi)

A = Effective cross-section area on each side of the piston (in^2)

Assuming the piston was displaced by Δx on one side, the volumes on each side of the cylinder V_1 and V_2 was expressed as shown in Equation 3.29 and 3.30.

$$V_1 = V_{in} - A\Delta x \qquad \text{Eqn. (3.29)}$$

$$V_2 = V_{in} + A\Delta x \qquad \text{Eqn. (3.30)}$$

The pressures one each side of the cylinder was expressed as shown in Equation 3.31.

$$P_1V_1 = P_2V_2 = P_{in}V_{in} = \text{constant} \qquad \text{Eqn. (3.31)}$$

Therefore, the pressure difference was expressed as ΔP.

$$\Delta P = P_1 - P_2 \qquad \text{Eqn. (3.32)}$$

$$\Delta P = P_{in}V_{in}\left(\frac{1}{V_{in} - A\Delta x} - \frac{1}{V_{in} + A\Delta x}\right) \qquad \text{Eqn. (3.33)}$$

$$\Delta P = \frac{2\,A\,P_{in}\,V_{in}}{{V_{in}}^2 - (A\,\Delta x)^2}\,\Delta x \qquad \text{Eqn. (3.34)}$$

The pressure difference induces a force $F = \Delta P(A)$, which was further expressed as in Equation 3.35.

$$F = \frac{2\,A^2\,P_{in}\,V_{in}}{{V_{in}}^2 - (A\,\Delta x)^2}\,\Delta x \qquad \text{Eqn. (3.35)}$$

But stiffness $K = F/\Delta x$. For sufficiently large plenums, it was assumed that $V_{in} \gg A\,\Delta x$.

$$K = \frac{2\,A^2\,P_{in}\,V_{in}}{{V_{in}}^2 - (A\,\Delta x)^2} = \frac{2\,A^2\,P_{in}}{V_{in}} \qquad \text{Eqn. (3.36)}$$

However, due to stiction within the cylinder and the slider, the inherent stiffness of the simulator was to be considered while calculating the equivalent cylinder pressure. The inherent stiffness of the system was measured to be 519.6278 N/m. The stiffness K in Equation 3.37 is the difference between the operator specific stiffness and the system inherent stiffness.

$$K = K_S - K_{inherent} \qquad \text{Eqn. (3.37)}$$

Therefore, the equivalent pressure for stiffness was expressed as shown in Equation 3.38.

$$P_{in} = \frac{(K_S - K_{inherent})\, V_{in}}{2\, A^2} \qquad \text{Eqn. (3.38)}$$

The equivalent pressure for each participant at each condition was calculated in Matlab and are presented in Section 4.1. The final developed model of the pistol grip tool simulator is shown in Figure 3.14.

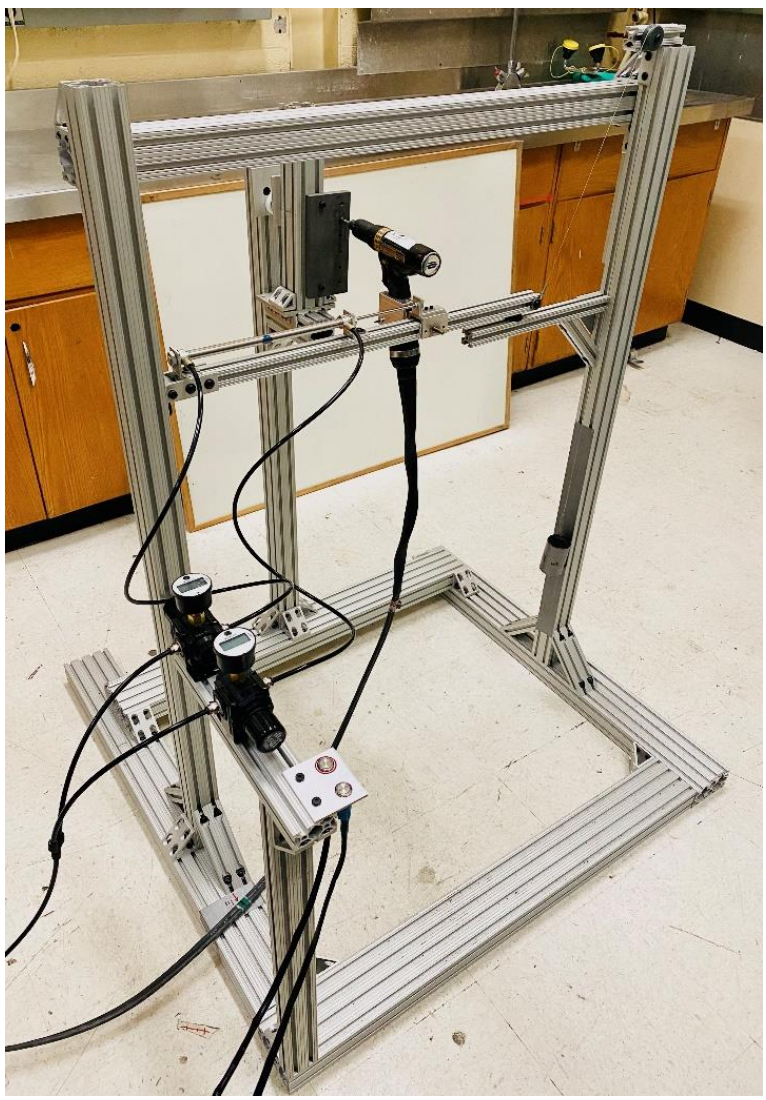

Figure 3.14: Pistol grip tool simulator

3.4 Design of Simulator Experiments

Finally, the simulator was fully developed and considered functional to simulate the dynamics of a human operator using a pistol grip tool. The performance of the simulator was evaluated, and results are presented in Section 4.2.

Furthermore, the simulator was used to test the effects of various parameters influencing the tool handle response. The angular displacement of the tool handle about the spindle axis was considered as the observed output parameter for each experimental condition. Two categories of test conditions were selected based on the capability of the simulator: namely the task conditions, and fastener conditions. The task conditions included variation in target torque, fastener location, and spindle operating speed. The fastener conditions included the fastener material, drive style, and fastener head type.

Target Torque

The in-vivo study considered 3 variations of target torque – 5, 7.5, and 10 Nm. Therefore, the effective stiffness of each participant was derived at each of these torques. It was observed that the simulator was capable of simulating the participants with reasonable accuracy at 5 and 7.5 Nm torques. However, the simulator failed to simulate the tool operation at 10 Nm. It was observed that the design elements in the simulator failed to meet the loading conditions experienced at 10 Nm. Specifically, the sleeve bearings failed, and the friction in the tool slider was significantly high. Therefore, the effects of varying the target torque between 5 and 7.5 Nm was tested for in this study.

Fastener Location

Similarly, four different fastener locations were tested for during the in-vivo study. Each of the four fastener locations were chosen such that they represented a unique orientation of the operator wrist during tool operation. This produced four unique effective stiffness values for each operator, at a given torque. Further, each stiffness value was converted to the cylinder pressure to emulate the muscular effort from the tool operator. The fastener locations being tested for, and their corresponding wrist orientations are summarized in Table 3.9.

Table 3.9: Fastener locations and corresponding wrist orientations

Fastener location	Wrist orientation
Low	Ulnar deviation – low
High	Ulnar deviation – high
Under	Radial deviation
Right	Flexion

The target torques and fastener locations were tested at the same experimental conditions of the in-vivo study and were thereby used to evaluate the performance of the simulator, as outlined in Section 4.2. It was observed that the simulator best emulated the dynamics of the human operator at 7.5 Nm torque. Therefore, the following experimental conditions were tested at a constant torque of 7.5 Nm to produce accurate, repeatable results.

Spindle Speed

The effects of spindle speed were tested by varying the operating speed of the tool. Five speeds were tested – 100, 120, 140, 160, and 180 RPM. However, it was observed that tool failed to complete the tasks successfully at 180 RPM due to an overload in the target torque. Therefore 180 RPM was neglected, and only four speeds were considered for this test condition.

Fastener Material

The effects of fastener material were tested by varying the material of the M6 × 1 mm, flat-head screw. A minimum of three material variations were considered for this study. However, it was found that three distinct materials with Torx Plus drive style was not commercially available. Alternatively, Hex drive style was chosen for all fasteners. The three materials considered in this condition are summarized in Table 3.10.

Table 3.10: Fastener material properties

Material	Finish	Elastic Modulus (GPa)
Alloy Steel	Black-oxide	200
18-8 Stainless Steel	Passivated	193
Brass	N/A	97

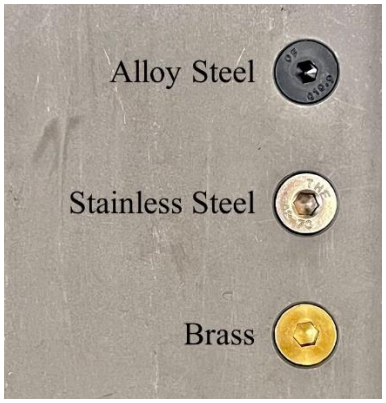

Figure 3.15: Fastener materials

Drive Style

Similarly, the effects of different drive styles were tested. It was found that only two drive styles were commercially available such that all other design specifications of the fastener remained constant. The two drive styles considered were Torx Plus – T30, and Hex – 4 mm, both of 1/4” Hex shank, and 2” length made of Steel for power tools. The fastener material for both styles was chosen to be Black-Oxide Alloy Steel.

Figure 3.16: Fastener drive styles

Fastener Head Type

Finally, the effects of different fastener head styles were tested. Two types of fastener head chosen were – Flat Head (with 90° countersink angle), and Button Head (with head height of 3.3 mm). Both fasteners were made of Black-Oxide Alloy Steel, and Hex – 4 mm drive style. Although the head shapes are different, it was observed that the fundamental difference was the contact surface dynamics between the joint plate and the fastener head. The Flat Head screw used a 45° conical frustum at the end of the threaded hole that made an inclined contact with the joint plate. Whereas the Button Head screw had a parallel planar contact with the joint plate.

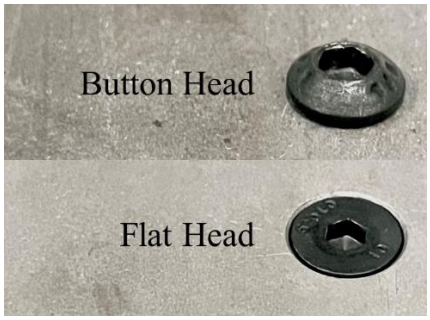

Figure 3.17: Fastener head types

Chapter 4

Results

The results of all experiments conducted are presented in this chapter. First, the operator parameters estimated from the in-vivo study are reported in Section 4.1. The performance evaluation of the simulator is presented in Section 4.2. Finally, the effects of various system parameters were tested on the tool simulator and their results are reported in Section 4.4 to Section 4.8.

4.1 In-Vivo Study

The in-vivo study was performed to estimate the operator characteristics involved in resisting the tool reaction during the tightening phase. The maximum angular displacement of the tool handle was measured when the fastener reached the maximum target torque. The mean effective stiffness from 3 trials were estimated from the analytical model presented in Section 3.1. The required equivalent cylinder pressure was calculated for the 3 torque values, and 4 fastener locations, and the results are summarized from Section 4.1.1 to Section 4.1.3.

4.1.1 Torque – 5 Nm

Table 4.1: In-vivo stiffness and pressure at 5 Nm, Low

Participant	Torque (Nm)	Angle (deg)	Mean Stiffness (N/m)	Pressure (psi)
S1	5.18	59.80	717.33	41.32
S2	5.13	58.90	847.49	68.53
S3	5.07	49.67	957.40	91.50
S4	5.42	34.86	1365.98	176.90
S5	5.23	55.58	895.65	78.59
S6	5.27	42.99	1203.14	142.87
S7	5.33	38.24	1283.97	159.76
S8	5.24	45.98	1095.27	120.32
S9	5.39	52.26	897.73	79.03
S10	5.36	37.11	1377.38	179.28
Mean	5.26	47.54	1064.13	113.81
SD	0.12	9.13	233.94	48.90

Table 4.2: In-vivo stiffness and pressure at 5 Nm, High

Participant	Torque (Nm)	Angle (deg)	Mean Stiffness (N/m)	Pressure (psi)
S1	5.32	61.05	720.26	41.93
S2	5.12	59.58	758.57	49.94
S3	5.24	43.91	1074.80	116.04
S4	5.21	47.32	925.77	84.89
S5	5.25	53.01	876.90	74.68
S6	5.17	39.49	1175.51	137.09
S7	5.16	37.91	1138.49	129.35
S8	5.21	39.00	1185.36	139.15
S9	5.34	54.70	855.82	70.27
S10	5.32	40.84	1097.74	120.83
Mean	5.23	47.68	980.92	96.42
SD	0.07	8.80	174.43	36.46

Table 4.3: In-vivo stiffness and pressure at 5 Nm, Under

Participant	Torque (Nm)	Angle (deg)	Mean Stiffness (N/m)	Pressure (psi)
S1	5.33	64.77	675.91	32.66
S2	5.22	54.08	870.86	73.41
S3	5.17	53.95	890.21	77.46
S4	5.20	35.95	1229.59	148.39
S5	5.29	43.28	1072.96	115.66
S6	5.25	36.29	1272.30	157.32
S7	5.36	41.19	1209.67	144.23
S8	5.34	41.75	1222.72	146.96
S9	5.37	44.18	1118.14	125.10
S10	5.37	37.11	1236.67	149.87
Mean	5.29	45.25	1079.90	117.11
SD	0.07	9.44	201.56	42.13

Table 4.4: In-vivo stiffness and pressure at 5 Nm, Right

Participant	Torque (Nm)	Angle (deg)	Mean Stiffness (N/m)	Pressure (psi)
S1	5.20	50.36	879.55	75.23
S2	5.42	51.55	846.64	68.35
S3	5.38	52.14	857.47	70.61
S4	5.30	39.72	1101.54	121.63
S5	5.20	50.50	963.73	92.82
S6	5.30	37.85	1173.27	136.62
S7	5.43	41.63	1142.21	130.13
S8	5.35	36.97	1368.60	177.45
S9	5.43	44.18	1083.50	117.86
S10	5.36	36.22	1302.48	163.63
Mean	5.34	44.11	1071.90	115.43
SD	0.09	6.48	183.44	38.34

4.1.2 Torque – 7.5 Nm

Table 4.5: In-vivo stiffness and pressure at 7.5 Nm, Low

Participant	Torque (Nm)	Angle (deg)	Mean Stiffness (N/m)	Pressure (psi)
S1	7.68	75.99	805.04	59.66
S2	7.63	75.55	861.54	71.47
S3	7.64	70.58	923.87	84.49
S4	7.94	52.50	1210.97	144.50
S5	7.85	68.06	890.00	77.41
S6	7.87	55.98	1151.35	132.04
S7	7.84	51.12	1269.19	156.67
S8	7.84	54.88	1157.23	133.27
S9	7.92	59.02	1009.78	102.45
S10	7.78	58.07	1115.62	124.57
Mean	7.80	62.17	1039.46	108.65
SD	0.11	9.48	162.47	33.96

Table 4.6: In-vivo stiffness and pressure at 7.5 Nm, High

Participant	Torque (Nm)	Angle (deg)	Mean Stiffness (N/m)	Pressure (psi)
S1	7.76	70.12	877.22	74.74
S2	7.66	72.56	842.83	67.55
S3	7.68	59.03	1121.94	125.89
S4	7.80	59.81	1054.63	111.82
S5	7.75	66.12	970.96	94.34
S6	7.75	60.50	1110.78	123.56
S7	7.80	54.35	1243.27	151.25
S8	7.77	50.49	1340.41	171.56
S9	7.57	66.03	983.83	97.03
S10	7.89	57.42	1150.24	131.81
Mean	7.74	61.64	1069.61	114.96
SD	0.09	6.97	156.41	32.69

Table 4.7: In-vivo stiffness and pressure at 7.5 Nm, Under

Participant	Torque (Nm)	Angle (deg)	Mean Stiffness (N/m)	Pressure (psi)
S1	7.66	82.89	686.38	34.85
S2	7.88	68.07	862.79	71.73
S3	7.73	61.67	1018.22	104.21
S4	7.90	54.17	1167.78	135.47
S5	7.78	52.88	1193.39	140.83
S6	7.88	46.20	1399.63	183.93
S7	7.72	57.73	1086.08	118.40
S8	7.83	49.18	1308.61	164.91
S9	7.81	61.00	1001.04	100.62
S10	7.76	48.72	1345.92	172.71
Mean	7.80	58.25	1106.99	122.77
SD	0.08	10.99	223.76	46.77

Table 4.8: In-vivo stiffness and pressure at 7.5 Nm, Right

Participant	Torque (Nm)	Angle (deg)	Mean Stiffness (N/m)	Pressure (psi)
S1	7.77	60.09	1025.32	105.70
S2	7.84	56.72	1035.27	107.78
S3	7.75	53.02	1164.38	134.76
S4	7.80	61.90	1097.87	120.86
S5	7.74	69.11	919.89	83.66
S6	7.75	46.55	1441.87	192.76
S7	7.76	50.53	1313.34	165.90
S8	7.76	45.31	1465.75	197.75
S9	8.04	50.39	1195.17	141.20
S10	7.83	43.28	1567.55	219.03
Mean	7.80	53.69	1222.64	146.94
SD	0.09	8.21	215.96	45.14

4.1.3 Torque – 10 Nm

Table 4.9: In-vivo stiffness and pressure at 10 Nm, Low

Participant	Torque (Nm)	Angle (deg)	Mean Stiffness (N/m)	Pressure (psi)
S1	10.29	76.01	979.32	96.08
S2	10.26	79.43	1011.23	102.75
S3	10.27	62.82	1277.49	158.40
S4	10.28	56.72	1460.87	196.73
S5	10.29	71.91	1054.65	111.83
S6	10.42	66.57	1131.62	127.92
S7	10.37	65.10	1216.61	145.68
S8	10.48	69.33	1094.95	120.25
S9	10.12	75.47	982.38	96.72
S10	10.38	65.98	1192.23	140.58
Mean	10.32	68.93	1140.13	129.70
SD	0.10	6.89	151.69	31.71

Table 4.10: In-vivo stiffness and pressure at 10 Nm, High

Participant	Torque (Nm)	Angle (deg)	Mean Stiffness (N/m)	Pressure (psi)
S1	10.23	78.43	1047.02	110.23
S2	10.20	85.26	902.80	80.09
S3	10.14	68.05	1263.90	155.57
S4	10.20	76.23	1027.54	106.16
S5	10.16	78.32	966.32	93.37
S6	10.24	63.96	1297.54	162.60
S7	10.20	73.36	1154.46	132.69
S8	10.25	66.63	1206.67	143.60
S9	10.16	85.76	947.52	89.44
S10	10.23	62.99	1272.31	157.32
Mean	10.20	73.90	1108.61	123.11
SD	0.04	8.30	148.04	30.94

Table 4.11: In-vivo stiffness and pressure at 10 Nm, Under

Participant	Torque (Nm)	Angle (deg)	Mean Stiffness (N/m)	Pressure (psi)
S1	10.28	62.93	1172.80	136.52
S2	10.21	75.96	1039.97	108.76
S3	10.30	77.01	999.18	100.23
S4	10.27	66.90	1118.60	125.19
S5	10.34	64.80	1213.35	145.00
S6	10.30	52.62	1538.48	212.96
S7	10.27	67.76	1204.92	143.24
S8	10.30	59.81	1291.22	161.28
S9	10.28	63.92	1207.99	143.88
S10	10.33	58.10	1335.81	170.60
Mean	10.29	64.98	1212.23	144.77
SD	0.04	7.52	153.99	32.19

Table 4.12: In-vivo stiffness and pressure at 10 Nm, Right

Participant	Torque (Nm)	Angle (deg)	Mean Stiffness (N/m)	Pressure (psi)
S1	10.34	72.99	1061.83	113.33
S2	10.12	82.37	997.18	99.82
S3	10.23	63.20	1246.74	151.98
S4	10.30	65.69	1158.84	133.61
S5	10.21	99.03	816.90	62.14
S6	10.33	54.05	1547.84	214.91
S7	10.26	72.34	1100.87	121.49
S8	10.44	59.85	1303.60	163.86
S9	10.37	65.93	1221.32	146.66
S10	10.41	50.15	1625.06	231.05
Mean	10.30	68.56	1208.02	143.88
SD	0.10	14.23	243.34	50.86

4.1.4 Subjective Ratings

The NASA TLX was used to assess the subjective workload experienced by the tool operators during the in-vivo study. The ratings from operators were weighted over six factors, and the mean values of all 10 participants were calculated. The ratings for each factor varied from a maximum of 100, to a minimum of 0. The results of the subjective ratings are summarized in Table 4.13.

Table 4.13: Subjective ratings of in-vivo experiments

Factor	S1	S2	S3	S4	S5	S6	S7	S8	S9	S10	Mean
Mental Demand	35	20	20	20	60	45	75	35	40	55	41
Physical Demand	85	60	40	25	40	40	65	50	35	60	50
Temporal Demand	25	25	20	20	25	40	15	35	40	15	26
Performance	70	55	35	0	70	20	10	25	70	5	36
Effort	85	30	15	55	45	35	50	15	55	40	43
Frustration	60	40	15	0	25	5	15	5	55	5	23
Weighted Rating	74	43	27	29	53	33	50	35	52	36	43

4.2 Performance Evaluation of Simulator

The parameters estimated from the in-vivo study were used to develop a functional tool simulator. The performance of the simulator was evaluated to assess the accuracy with which the simulator emulates the tool handle response. Therefore, the angular displacement of the tool handle was chosen to assess the simulator performance. An unpaired t-test was used to compare the mean angles between the in-vivo trials and the tool simulator. A Shapiro-Wilk normality test was used to determine if the data was normally distributed. Since the simulator was not tested at 10 Nm, only the angles at 5 Nm and 7.5 Nm were compared.

5 Nm Torque

Table 4.14: Difference between in-vivo and simulator experiments at 5 Nm

Participant	In-Vivo (deg)	Simulator (deg)	Mean Difference
S1	59.00	48.58	10.42
S2	56.03	43.64	12.38
S3	49.92	43.02	6.89
S4	39.46	40.81	-1.35
S5	50.59	42.43	8.16
S6	39.15	39.63	-0.47
S7	39.74	40.73	-0.98
S8	40.92	40.63	0.30
S9	48.83	41.71	7.12
S10	37.82	41.05	-3.23
Mean	46.15	42.22	3.92
SD	7.71	2.54	5.64

The unpaired t-test at 5 Nm showed that the two-tailed p-value was 0.14. The mean difference between the operators and simulator was found to be 3.92°. Further, the t-value was found to be 1.53, and the standard error of difference was 2.57. The normality tests did not show a significant deviation from the normal distribution.

7.5 Nm Torque

Table 4.15: Difference between in-vivo and simulator experiments at 7.5 Nm

Participant	In-Vivo (deg)	Simulator (deg)	Mean Difference
S1	72.27	61.03	11.24
S2	68.22	61.59	6.63
S3	61.07	57.88	3.20
S4	57.10	56.15	0.94
S5	64.04	60.95	3.09
S6	52.31	58.12	-5.82
S7	53.43	57.77	-4.34
S8	49.97	51.30	-1.34
S9	59.11	60.80	-1.68
S10	51.87	59.09	-7.21
Mean	58.94	58.47	0.47
SD	7.47	3.09	5.75

The unpaired t-test at 7.5 Nm showed that the two-tailed p-value was 0.86. The mean difference between the operators and simulator was found to be 0.47°. Further, the t-value was found to be 0.18, and the standard error of difference was 2.56. The normality tests did not show a significant deviation from the normal distribution.

4.3 Target Torque

After verifying the accuracy of the tool simulator, it was used to simulate each participant from the in-vivo study. In this section, the angular displacement values of all four fastener locations were averaged at each torque. The typical values of mean angular displacement at 5 Nm and 7.5 Nm are shown in Figure 4.1.

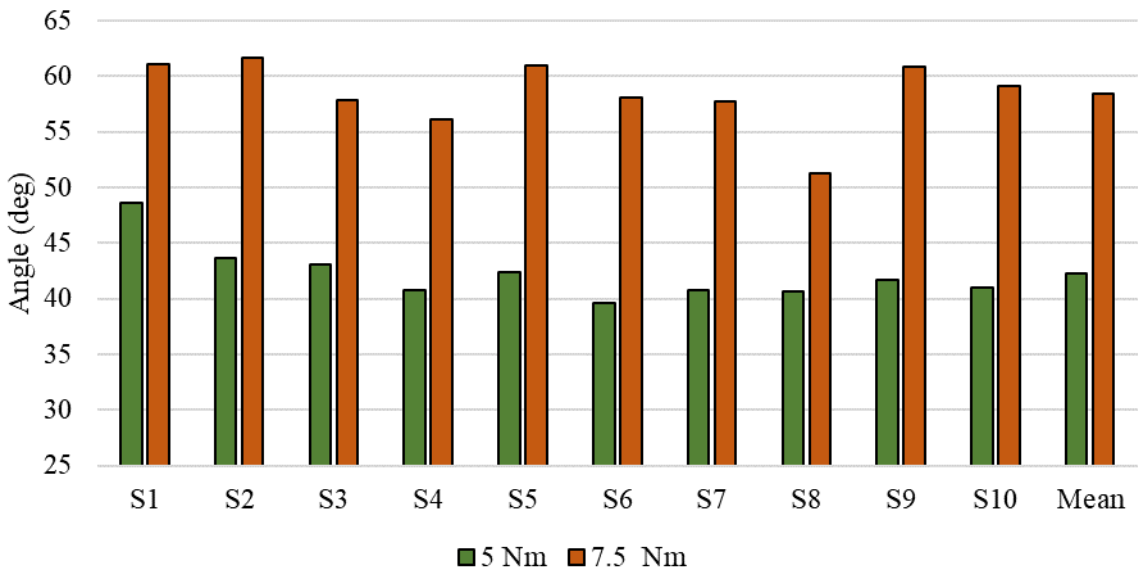

Figure 4.1: Effects of variation in target torque

At 5 Nm, the mean angular displacement was found to be 42.22° (SD = 2.54). Whereas at 7.5 Nm, the mean angular displacement was found to be 58.47° (SD = 3.09).

4.4 Fastener Location

Four different fastener locations, each corresponding to different orientations of the wrist were simulated. The angular displacement results of all 10 participants and their mean values at 5 Nm torque are reported in Figure 4.2.

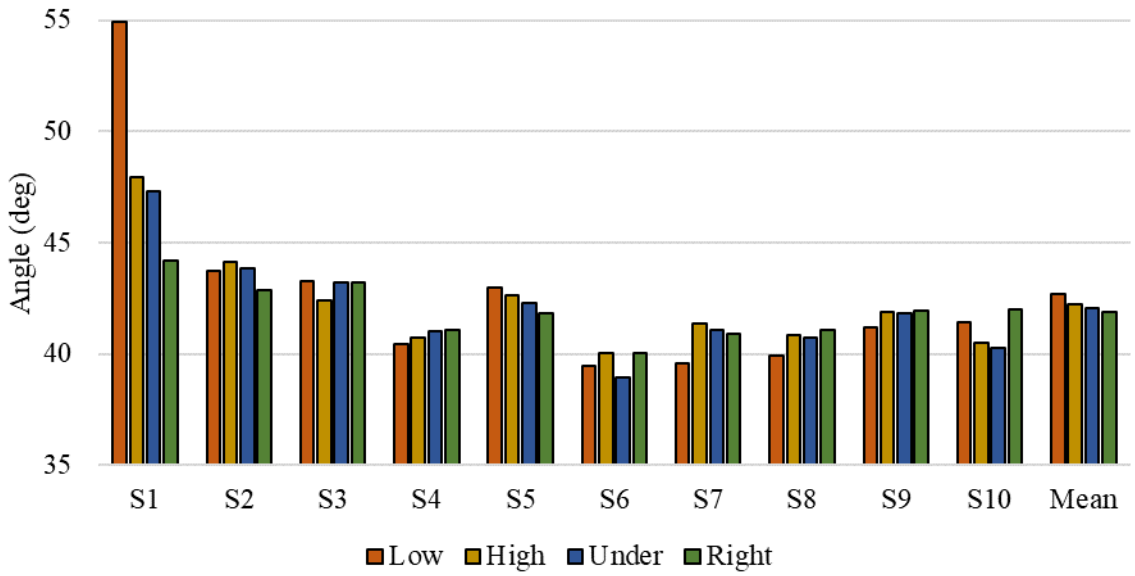

Figure 4.2: Effects of variation in fastener location at 5 Nm

The mean angular displacement was found to be maximum (42.70°) at the 'Low' position, whereas it was minimum (41.91°) at the 'Right' position.

Similarly, the angular displacement results of all 10 participants and their mean values at 7.5 Nm torque are reported in Figure 4.3.

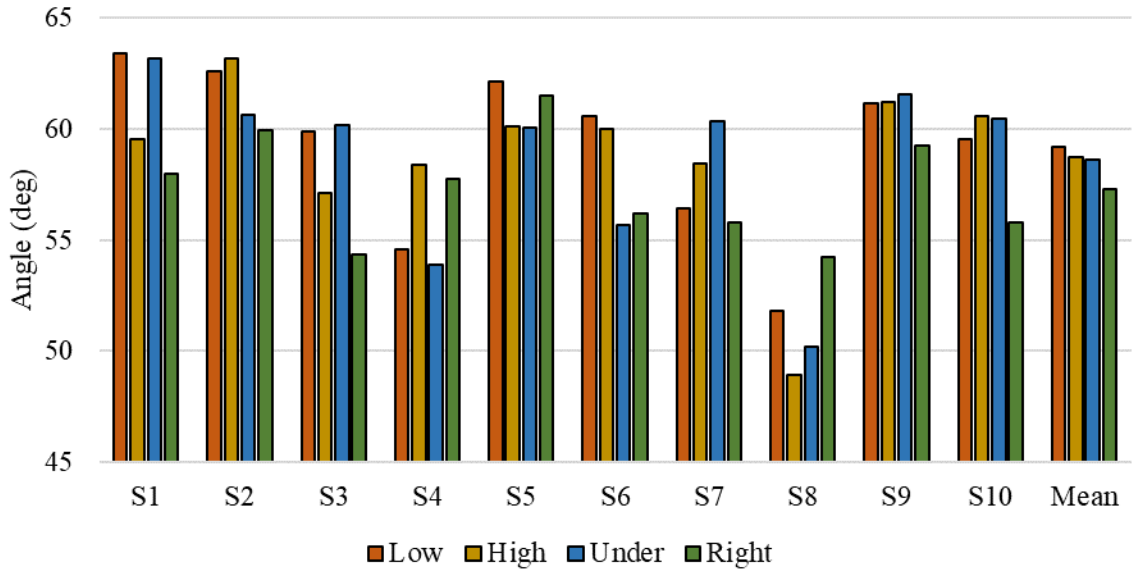

Figure 4.3: Effects of variation in fastener location at 7.5 Nm

The mean angular displacement was found to be maximum (59.22°) at the 'Low' position, whereas it was minimum (57.28°) at the 'Right' position.

4.5 Spindle Speed

The mean angular displacements of the tool handle at four different spindle speeds were extracted. The torque buildup time from the start of the tightening phase till the target torque was also recorded. The results are shown in Figure 4.4.

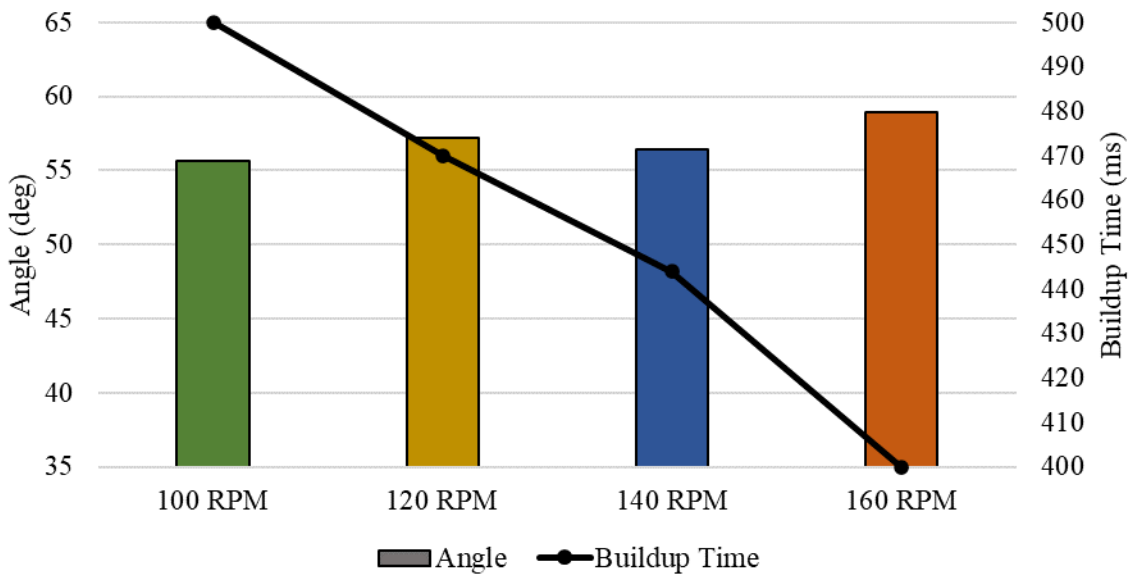

Figure 4.4: Effects of variation in tool spindle speed

The speeds varied as 100, 120, 140, and 160 RPM. The resulting mean angular displacement was 57.04°, with a standard deviation of 1.41. The torque buildup times were found to be 500, 470, 444, and 400 milliseconds, respectively.

4.6 Fastener Material

Three fastener materials – Alloy Steel, Stainless Steel, and Brass were tested at 7.5 Nm torque, and their mean angular displacements are reported. The elastic modulus of each material was used for comparison and is also reported in Figure 4.5.

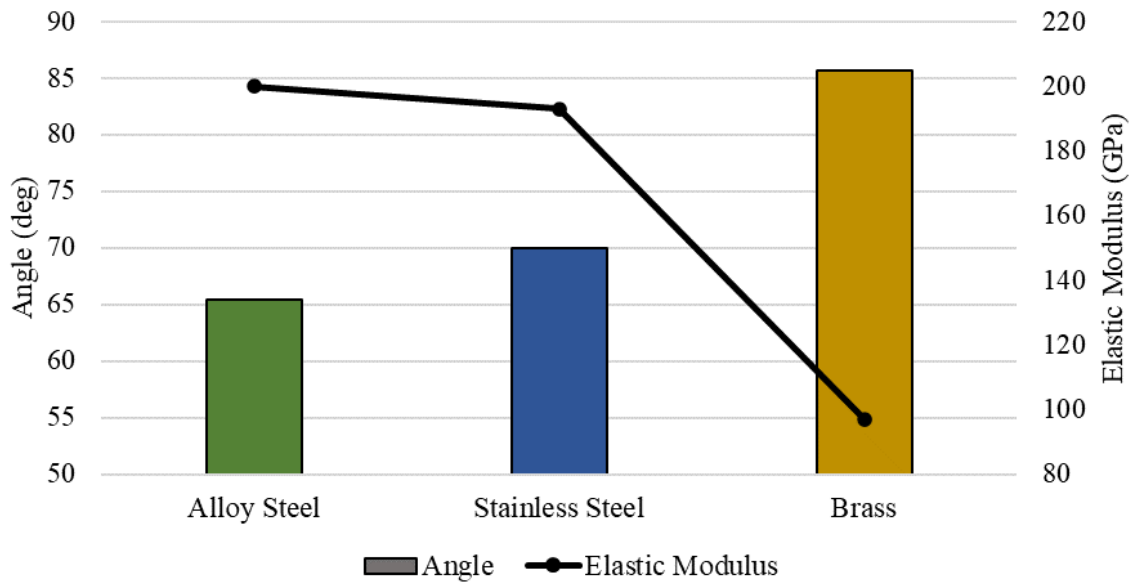

Figure 4.5: Effects of variation in fastener material

4.7 Drive Style

The mean angular displacements of two fastener drive styles – Torx Plus and Hex are reported in Figure 4.6.

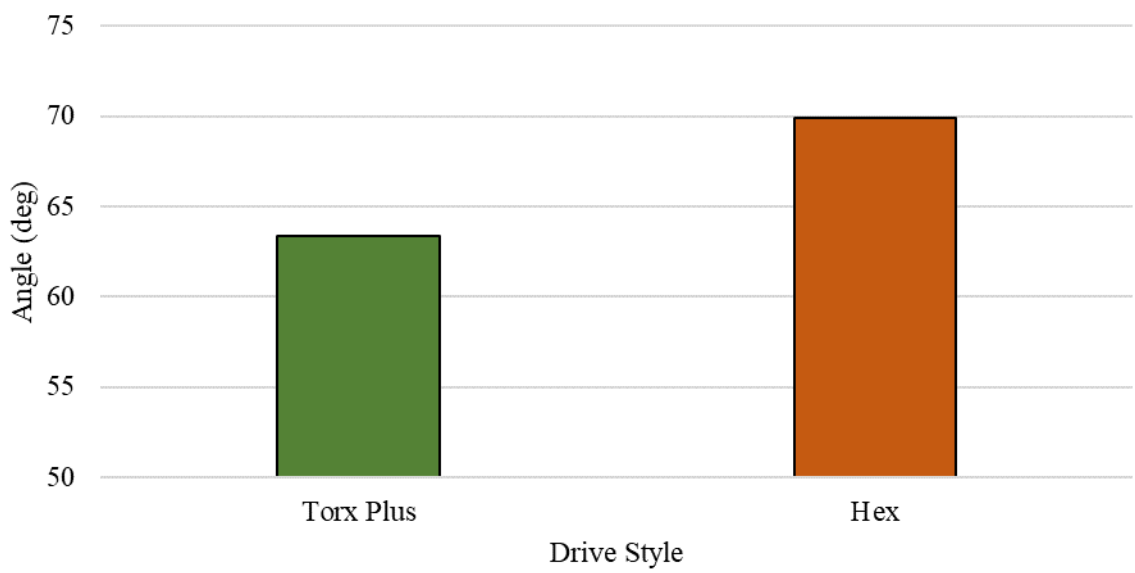

Figure 4.6: Effects of variation in fastener drive style

4.8 Fastener Head Type

Finally, the mean angular displacements of two fastener head types – Flat Head and Button Head are reported in Figure 4.7.

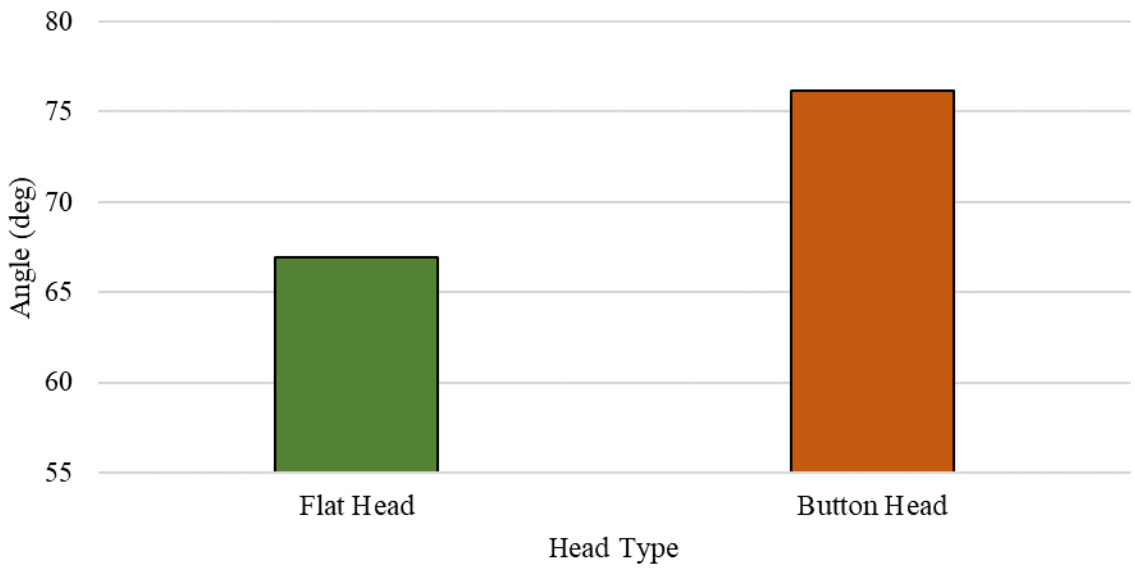

Figure 4.7: Effects of variation in fastener head type

Chapter 5

Discussion

The current study investigated the effects of various tool, task, and operator parameters to mitigate injuries that arise from the tool handle displacement during tightening. This was achieved by modelling the system analytically, and further developing a test rig to simulate the dynamics of tool operation and testing each parameter. In this chapter, the results of the investigation carried out are discussed and partially validated in comparison with previous literature. Sufficient literature on the current tool type and power source was not available to exactly validate the models. Therefore, results observed in this study were established for a pistol grip tool with cabled electric power. The corresponding optimum conditions required to minimize the tool handle displacement were identified and are presented in this chapter.

5.1 Analytical Model

In Section 3.1, the pistol grip tool and human operator dynamic system was represented with an analytical model to provide a numerical estimation of tool handle responses during tightening tasks. Initially, the system parameters were identified and taken into consideration while developing the model. It was found that the tool related variables such as mass moment of inertia played a significant role in predicting the dynamic response of the tool handle. However, it was also shown that the task and operator related variables were also involved in tool handle dynamics. Each of the system variables were modelled and measured individually, and later incorporated in the analytical model.

The system was simplified to a single degree of freedom torsional model with spring, mass, damper elements. An inverse dynamic equation of motion was derived to predict the effective stiffness and damping of individual tool operators. But the equation required a measurement of the mass moment of inertia of the system. The mass moment of inertia of the tool and operator were estimated individually through experiments. In this study, the mass moment of inertia of the pistol grip tool with cable about the spindle axis was found to be 0.01023 kgm^2. Lin et. al. (2003b) measured the mass moment inertia of two pistol grip tools – battery and pneumatic powered, as shown in Table 5.1. In comparison with the current values, it was observed that the order of magnitude of these tools were similar. However, the difference in values is attributed to difference in shape as well as cable mass. The battery-powered tool had a significantly higher mass at the end of the tool handle, whereas the pneumatic tool had a relatively lighter pipe supplying air at the end of the handle. The mass of the current cable is assumed to be ranging in between these and the

inertial value reflects. Therefore, it was assumed that the bifilar and simple pendulum experiments provided a reasonably accurate measurement of mass moment of inertia of the tool.

Table 5.1: Mass moment of inertia of pistol grip tools

Tool	Power Source	Mass Moment of Inertia (kgm^2)
Current	Electric (cable)	0.01023
Lin et. al., (2003b)	Battery	0.04390
Lin et. al., (2003b)	Pneumatic	0.00520

Further, an in-vivo study involving experienced tool operators was conducted at the Honda of Canada Manufacturing assembly plant. The mean body weight of the study group was found to be 84 kgs, and the mean mass moment of inertia of the entire tool and operator system was calculated to be 0.01431 kgm^2. The torque and angular displacement measurements were derived from the tool controller software. Finally, the inverse dynamic equation was used to estimate the effective stiffness values of all ten participants from the in-vivo study. The effective damping was assumed to be negligible and neglected in evaluating the inverse dynamic equation.

Three different torque levels – 5, 7.5, 10 Nm were compared. Each torque level was operated at four different fastener locations and averaged between all trials. The mean effective stiffness at each target torque is shown in Table 5.2.

Table 5.2: Mean stiffness at various torques

Torque (Nm)	Mean Stiffness (N/m)	Angle (deg)	Displacement (mm)
5	1049.21	46.15	72.49
7.5	1109.67	58.94	92.59
10	1167.25	69.09	108.53
Mean	1108.71	58.06	91.20

It was estimated that the mean stiffness of all operators was 1108.71 N/m. The value was validated by comparing them to those reported in previous literature. Lin et. al., (2005) predicted that the mean operator stiffness was 1126.80 N/m. It was observed that the current method of predicting operator characteristics was reasonably accurate. However, the differences in these values are attributed to the difference in the operating torque, speed as well as fastener locations. Moreover, the mean values also vary depending on the population group chosen. Lin et. al. (2005) considered 13 females and 12 males, whereas the current

study considered 8 males and only 2 females. Discrepancies could be due to the gender population ratio chosen for the study. Nonetheless, the current predicted values were considered accurate and used to represent the operator characteristics.

Further, the displacement of the tool handle was compared. The linear displacement of the tool handle at the center of pressure (l_{COP} = 90 mm) was calculated as the arc length of its angular displacement, as shown in Table 5.2. The mean handle displacement was calculated to be 91.20 mm; whereas Lin et. al., (2005) predicted the mean handle displacement as 79.92 mm. The differences are primarily due to the varying tool shape, torque level, and hand gripping positions.

Based on the current findings, it can be said that the analytical model presented in Section 3.1 represented the pistol grip tool–operator system with reasonable accuracy. The single degree of freedom assumption was found to be sufficient in modelling the system and predicting the operator responses to handle reaction.

Results from the in-vivo study also provided further insight into the mean handle responses at various fastener locations (Table 4.1 to Table 4.12). At 5 Nm torque, it was observed that the High position (ulnar deviation – high) produced the highest displacement, whereas Right position (wrist flexion) produced the least. At 7.5 Nm, it was observed that the Low position (ulnar deviation – low) produced the highest displacement, whereas Right position (wrist flexion) produced the least. And at 10 Nm, High position (ulnar deviation – high) produced the highest displacement, whereas Under position (radial deviation) produced the least. Therefore, on an average, it was observed that wrist ulnar deviation resulted in the most displacement of the tool handle, and wrist flexion resulted in the least displacement of the handle.

Further, subjective ratings of participants were recorded with the NASA Task Load Index, shown in Table 4.13. The survey found that physical demand (50) was the most contributing factor to perceived poor performance, followed by effort (41). This is possibly due to the large loads experienced by the participants and the voluntary muscle effort needed to resist handle reactions. It was also found that frustration (23) was the least contributing factor to perceived poor performance, followed by temporal demand (26). This is possibly due to the impulsive, short durations of the loads experienced and frequent breaks, as opposed to continuous exposure.

5.2 Pistol Grip Tool Simulator

A pistol grip tool simulator was designed and developed to emulate the tool handle reaction during a typical fastening operation. Several elements were incorporated into the design such that the simulator dynamics mimicked humans with reasonable accuracy. The stiffness values measured from the in-vivo were translated into equivalent pressure of the pneumatic actuator. The performance of the simulator was evaluated in Section 4.2 by comparing the angular displacements of tool handle with the in-vivo trials. At

5 Nm torque, the unpaired t-test showed that the mean difference between the two studies was statistically insignificant ($p = 0.14$), with a mean difference in prediction of 3.92°. While the error was relatively low, it was observed that the simulator performed even better at 7.5 Nm. At 7.5 Nm torque, the unpaired t-test showed that the mean difference between the two studies was 0.47°, which is also statistically insignificant ($p = 0.86$). Therefore, it was concluded that the designed simulator emulated the tool dynamics most accurately at 7.5 Nm. Since the simulator was required to investigate several other parameters, it was also required to test for these conditions at a fixed torque such that it produced observable, repeatable results. Hence, 7.5 Nm was chosen to be the appropriate torque level.

5.3 Target Torque

Initially, the effect of target torque on the handle displacement was tested. It was observed in Figure 4.1 that when the torque increased from 5 Nm to 7.5 Nm, the angular displacement also increased by 38.5%. This showed that the handle displacement was directly proportional to the applied target torque. This is also in agreement with general mechanics – the motion of an object is directly proportional to the force applied, and the proportionality constant is called object's stiffness. Although using a lower torque may reduce handle displacements, it may not be practicable as the target torque is typically a design requirement for the fasteners used. However, if the design permits the use of lower torques, it may be beneficial to do so in order to reduce the handle displacement.

5.4 Fastener Location

Workers in assembly lines tighten fasteners in various locations, some being inaccessible, or requiring them to grip the tool in awkward hand positions. Therefore, the effects of wrist orientations were tested in the simulator. The mechanism of the simulator doesn't allow to simulate the actual orientation of the wrist itself, however it is capable of simulating the effective stiffness of the operator at each wrist orientation. The effective stiffness at four fastener locations, each corresponding to a unique wrist orientation as shown in Table 3.9, was estimated from the in-vivo study (Section 4.1).

The resulting mean angular displacements from each location were measured at 5 Nm (Figure 4.2), and 7.5 Nm (Figure 4.3). The trends from both torques agreed with each other. It was shown that ulnar deviation of the wrist produced the highest angular displacement. Therefore, it can be said that ulnar deviation of the wrist provides the least stiffness (or resistance) to tool handle reaction. It is also important to note that, for right-handed operators in neutral position, the pistol grip handle reaction primarily produces a wrist pronation movement. Therefore, it is further elucidated that a combination of ulnar deviation and wrist pronation is considered least safe during pistol grip tool operation.

Meanwhile, it was also shown that wrist flexion produced the least angular displacement. However, during wrist flexion, the handle reaction does not pronate the wrist a lot. Instead, it was observed to primarily cause wrist extension. Therefore, it can be inferred that flexion-extension of the wrist produces the highest stiffness during tool handle reaction.

Therefore, it was found that improvements could be made with regards to wrist orientations relative to the fastener location such that they produce the least handle displacement. Operators could undergo training to adopt safer ergonomic strategies, thereby mitigating repetitive strain injuries.

5.5 Spindle Speed

The operational speed of the tool spindle varied between 100 RPM to 160 RPM with increments of 20 RPM, and the angular displacement of the handle was observed, as shown in Figure 4.4. The mean angular displacement of all four speeds was 57.04° (SD = 1.4), which showed that there was no significant influence on the handle response due to change in speeds. However, it was seen that the torque build-up durations changed significantly. When the speeds were increased from 100, 120, 140, to 160 RPM, the buildup time reduced from 500, 470, 444, and 400 ms respectively. Therefore, for every increment of 20 RPM in the spindle speed, the torque build-up time reduced by 7.1% on an average.

Although the speed had no significant effect on the peak angular displacement of the handle, the duration of the torque build-up phase may affect the muscle contraction dynamics. Shorter durations of handle reaction demand an even faster reaction response from the muscles opposing handle motion. Such impulsive forces could have negative consequences on the forearm muscles; however, it was not tested in this study.

5.6 Fastener Material

The angular displacements resulting from the use of three different fastener materials were compared, as shown in Figure 4.5. The elastic modulus of each material was taken into consideration while comparing their behaviors. It was observed that brass, with the lowest elastic modulus of 97 GPa, produced the highest angular displacement of 85.70° (SD = 1.35). Meanwhile, stainless steel with an elastic modulus of 193 GPa produced an angular displacement of 70.00° (SD = 1.21). Whereas alloy steel had the highest elastic modulus of 200 GPa and produced the lowest angular displacement of 65.37° (SD = 0.99). This showed that a 99% increase in the elastic modulus resulted in reduction of the angular displacement by 18.3%. Similarly, an increase in the elastic modulus by 3.6% resulted in reduction of the angular displacement by 6.6%. Therefore, it was inferred that the angular displacement of the tool handle was inversely proportional to the elastic modulus of the fastener material.

This can be further explained by considering the modulus of rigidity of the fasteners. The angle of twist, φ, for a given applied torque is given by Equation 5.1.

$$\varphi = \frac{T\,L}{J\,G} \qquad \text{Eqn. (5.1)}$$

Where, T is the applied torque, L is the length of the fastener, J is the polar moment of inertia of the fastener, and G is the modulus of rigidity (shear modulus) of the fastener material. It can be assumed that T, L, and J are the same for all three fastener materials due to their identical geometry. Therefore, it was observed that the angle of twist is inversely proportional to the modulus of rigidity of the material. Table 5.3 outlines the modulus of rigidity of the three fastener materials considered.

Table 5.3: Modulus of rigidity of fastener materials

Material	Modulus of rigidity (GPa)
Alloy Steel	80
Stainless Steel	77
Brass	41

The angle of twist was approximated mathematically for all three materials. It was found that an 88% increase in the shear modulus resulted in a 46.7% decrease in the angle of twist. Also, a 4% increase in the shear modulus resulted in a 3.8% decrease in the angle of twist. It was seen that this trend is similar to the one observed when considering the modulus of elasticity. Therefore, the differences in the angular displacement of different materials can be attributed to their differences in the elastic and plastic deformations.

With the goal of reducing the angular displacement, fastener materials can be chosen appropriately based on their elastic and shear modulus. Although fastener materials such as brass are not commonly used, improvements can be made with common materials such as steel and aluminum. It could be beneficial to consider different alloy compositions and grades of similar materials when designing fastener specifications. While fastener materials could be optimized, considerations can also be made with regards to the material of the threaded hole components.

5.7 Drive Style

Two drive styles – Torx Plus and Hex were compared at similar test conditions, as shown in Figure 4.6. Hex drive produced a greater angular displacement of 69.93° (SD = 2.19). Whereas Torx Plus produced a relatively lower angular displacement of 63.36° (SD = 1.03). This showed a percentage decrease in the tool

response by 9.4% from Hex to Torx Plus. This is attributed to the geometrical advantage of Torx Plus over the Hex drive. Specifically, Torx Plus consists of a larger contact area between the driving bit and the fastener head. This results in more efficient energy absorption during the tightening phase. Furthermore, the angle between the contact surface of the driver and fastener, and the direction of the applied torque is greater in Torx Plus compared to that of Hex, as shown in Figure 5.1. This allows for a higher torque to be delivered to the fastener, while also wear and tear of the fastener. Therefore, it was inferred that drive styles with larger contact area between the driver and fastener produced smaller tool responses.

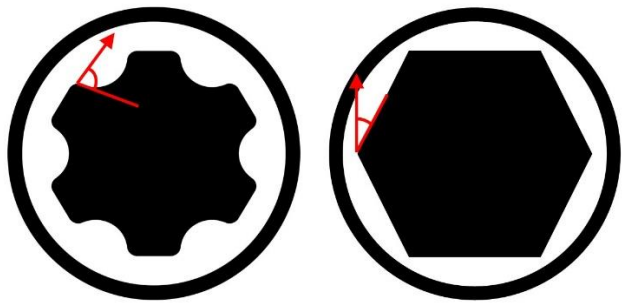

Figure 5.1: Contact planes of Torx Plus and Hex

Although the two most commonly used drive styles were tested, it was found that more unique styles were not commercially available while all other design specifications were constant. There is not much significance in using drives styles with lower contact surfaces than Hex since it is the most commonly used style among power tools. However, considerations can be made by using improvised Torx screws. For example, based on the current findings, it is expected that Torx Plus performs better than a conventional Torx drive. Torx Plus consists of flatter corners, thus allowing for higher torque transmission and minimized wear. Therefore, if possible, further design improvements can be made to Torx Plus such that the tool handle displacement is minimized.

5.8 Fastener Head Type

Finally, the performance of two fastener head types – Flat Head and Button Head were compared, as shown in Figure 4.8. Results showed that Button Head fasteners had a significantly higher angular displacement of 76.20° (SD = 1.13), whereas Flat Head fasteners performed better with a lower angular displacement of 66.93° (SD = 0.75).

The performance improvement in Flat Head fasteners is attributed to their larger contact area between the head and the joint plate. For the Flat Head screws used in this study, the lateral surface area of the chamfered region that was in contact with the joint plate was calculated to be 160.6 m^2. Whereas the contact area

between the underside annulus of the Button Head and joint plate was calculated to be 58.3 mm^2. Therefore, it was seen that a reduction in the surface contact area between the joint plate and fastener head by 63.7% increased the tool handle response by 13.8%. This showed that the tool handle response is inversely proportional to the contact area between the fastener and the joint plate.

5.9 Summary

Finally, the optimum conditions required to minimize the tool handle displacement were investigated. It was identified that the tool variables could be optimized by considering the lowest permissible torque and highest operating speed such that it does not result in torque overload. The operator variables could be optimized by orienting the wrist such that it provides the maximum stiffness at a given fastener location. Further, task related optimization includes using the stiffest fastener material, largest drive style, and widest fastener head type. Therefore, a combination of all these optimized parameters would result in the least possible handle displacement.

Chapter 6

Conclusion

6.1 Summary

The objective of the current study was to model the handle displacement of a DC-powered pistol grip hand tool during tightening tasks and optimize the operating conditions that minimize the handle displacement. This was carried out by implementing several methods to accurately model the system. Initially, a scoping review of various literatures evaluating the risk of injury and musculoskeletal disorders arising from hand tool usage was carried out. Important reactions parameters and their relationship with fastening operations were explored. Several gaps were identified and were taken into consideration in devising a methodology.

First, parameters within the system that influence tool handle displacement were identified. A single degree-of-freedom mechanical torsional model was used to represent the rotational motion of the tool handle displacement. Experiments were performed to measure each parameter within the proposed model. The mass moment of inertia of the pistol grip tool was approximated. Further, an inverse dynamic approach was used to estimate the remaining parameters in the model. Specifically, the effective stiffness of tool operators was established from an in-vivo study. The typical ranges of operator characteristics were measured from experienced tool operators working in an assembly line environment. Experimental data was extracted at various fastener locations and target torque levels. It was concluded that the single degree-of-freedom model was successful in estimating the operator characteristics involved in resisting tool handle displacement.

Furthermore, an ergonomic simulator of the pistol grip hand tool was designed and developed. The simulator successfully incorporated the parameters identified in the analytical model. The functional requirements of the simulator were identified based on the need to capture the interaction between the tool and operator hand. A quick-return mechanism was chosen to represent the single degree of freedom rotation about the spindle axis, as well as allow for an actuator to simulate the resistance offered by operators against the tool handle. Several other design elements ensured the accuracy of simulating the dynamic interaction as well. A pneumatic actuator was devised to represent the effective stiffness of tool operators, and their equivalent pressure values were derived. Finally, the pistol grip tool simulator was effectively developed, and its performance was evaluated. Results showed the simulator emulated a human operator with reasonably good accuracy and was therefore regarded fit to test the effects of several system parameters.

System parameters, broadly classified as tool, task, and operator related variables were tested on the tool simulator. The angular displacement of the tool handle was observed, and the optimum conditions that minimize the handle displacement were identified. Tool-related optimizations including the target torque and spindle speed were suggested. Task-related optimization included suggestions to various wrist orientations and fastener locations. Finally, recommendations were made on the design of fastener specifications. This included the fastener materials, drive styles, and fastener head types. Therefore, it is concluded that a combination of these optimized parameters would result in minimizing the tool handle displacement. This provides tool manufacturers and Occupational Health and Safety practitioners with an overview to establish standard guidelines and industrially applicable recommendations to mitigate injuries related to torque tool usage.

6.2 Limitations and Future Work

Although the proposed objectives were met, the current study posed several limitations and showed encouragement for future improvements.

1. The analytical model considered is linear in nature. However, the human muscle responses are naturally non-linear in nature. Future studies could model non-linearity.
2. The analytical model was simplified to just one degree-of-freedom. However, the actual reaction motion of the tool body is more than just one degree-of-freedom. Considering other axes of rotation could be beneficial in predicting operator parameters such as stiffness and damping more accurately.
3. Some previous studies neglected the mass moments of inertia of tool parameters such as cables and pipes. Although the current study addresses these issues by taking them into consideration, it was still an approximation, and an accurate method of measurement was not used. A more advanced method of measurement, as opposed to free oscillation methods, is required to calculate the mass moments of inertia.
4. The effective damping of the operators was assumed to be negligible and therefore neglected in evaluating the inverse dynamic equation of motion. Further studies can use least squares method to solve the overdetermined system of equations and predict the effective damping values.
5. Since the effective damping of operators was not estimated, it was also not incorporated into the simulator design. Improvements to the simulator can be made by including separate dampers such as electrorheological fluid (ERF) dampers. Further, inherent stiffness and damping of the simulator could be improved by reducing the friction of movable parts.

6. The current study tested only four fastener locations and three torques. Considering more locations and torques could provide further insight into the injury mechanism. Future tests could test for improvements to tightening algorithms and torque profiles.
7. The parametric study was limited to only three fastener materials, two drives styles, and two head types. Although the current study provided some insight into these parameters, a complete understanding of their behavior still lacks.
8. In future studies, the effect of joint plate material could be tested. An alternative to elastic modulus, such as hardness, density, etc. could be considered in comparing different materials.
9. Further insight could be gained by modelling the contact dynamics between the driver, fastener, and joint plate. Other drive style variations such as internal to external also require further examination.
10. Future studies could also include testing different fastener head profiles (heights). The current study did not test the effects of washers and sealing rings between the joint plate and fastener, and future studies could make these considerations.

References

[1] Lin, J. H., Radwin, R. G., Richard, T. G. (2001). Dynamic biomechanical model of the hand and arm in pistol grip power handtool usage. Ergonomics, Vol. 44, No. 3, 295-312.

[2] Lin, J. H., Radwin, R. G., Richard, T. G. (2003a). A single-degree-of-freedom dynamic model predicts the range of human responses to impulsive forces produced by power hand tools. Journal of Biomechanics, 36, 1845-1852.

[3] Lin, J. H., Radwin, R. G., Richard, T. G. (2003b). Handle dynamics predictions for selected power hand tool applications. Human Factors, Vol. 45, No. 4, 645-656.

[4] Lin, J. H., Radwin, R. G., Nembhard, D. A., (2005). Ergonomics applications of a mechanical model of the human operator in power hand tool operation. Journal of occupational and environmental hygiene, 2:2, 111-119.

[5] Lin, J. H., McGorry, R. W., Chang, C. C., Dempsey, P. G. (2007a). Effects of user experience, working posture and joint hardness on powered nutrunner torque reactions. Ergonomics, Vol. 50, No. 6, 859-876.

[6] Ku, C., Radwin, R. G. (2007). Power hand tool kinetics associated with upper limb injuries in an automobile assembly plant. Journal of occupational and environmental hygiene, 4: 391-399.

[7] Lin, J. H., McGorry, R. W., Banks, J. J. (2010a). Exposures and physiological responses in power tool operations: fastening vs unfastening threaded hardware. Journal of occupational and environmental hygiene, 7: 290-297.

[8] Lin, J. H., McGorry, R. W., Chang, C. C. (2007b). Hand-handle interface force and torque measurement system for pneumatic assembly tool operations: suggested enhancement to ISO 6544. Journal of occupational and environmental hygiene, 4: 332-340.

[9] Kihlberg, S., Kjellberg, A., Lindbeck, L. (1995). Discomfort from pneumatic tool torque reaction: acceptability limits. International Journal of Industrial Ergonomics, 15, 417-426.

[10] Lin, J. H., Maikala, R. V., McGorry, R., Brunette, C. (2010b). NIRS application in evaluating threaded fastener driving assembly tasks. International Journal of Industrial Ergonomics, 40, 146-152.

[11] Steingraber, C., Devries, D., Eaton, L., Smets, M., Stephens, A., Malone, G., Porto, R., Cort, J. (2021). Physical demands associated with right angle direct current power tools: an evaluation of current technology. Applied Ergonomics, 93, 103374.

[12] Kihlberg, S., Kjellberg, A., Lindbeck, L. (1993). Pneumatic tool torque reaction: reaction forces, displacement, muscle activity and discomfort in the hand-arm system. Applied Ergonomics, 24(3), 165-173.

[13] Lin, J. H., McGorry, R. W. (2008). Predicting subjective perceptions of powered tool torque reactions. Applied Ergonomics, 40, 47-55.

[14] Lin, J. H., McGorry, R. W., Maikala, R. V. (2012). The effects of joint torque, pace and work:rest ratio on powered hand tool operations. Ergonomics, Vol. 55, No. 3, 361-370.

[15] Mazaheri, A., Rose, L. M. (2021). Reaction load exposure from handheld powered tightening tools: A scoping review. International Journal of Industrial Ergonomics, 81, 103061.

[16] Ay, H., Luscher, A., Sommerich, C. (2010). Design and development of a torque tool testing rig that simulates human operator tool task interactions. Proceedings of the human factors and ergonomics society, 54th annual meeting.

[17] Ay, H., Luscher, A., Sommerich, C. (2013). Linear modeling of human hand-arm dynamics relevant to right angle torque tool interaction. Human Factors and Ergonomics Society. Vol. 55, No. 5, 893-910.

[18] Lin, J. H., McGorry, R. W., Chang, C. C., Dempsey, P. G. (2006). Handle displacement and operator responses to pneumatic nutrunner torque buildup. Applied Ergonomics, 37, 367-376.

[19] Oh, S.A., Radwin, R. G. (1997). The effects of power hand tool dynamics and workstation design on handle kinematics and muscle activity. International Journal of Industrial Ergonomics, 20, 59-74.

[20] Lin, J. H., Radwin, R. G., Fronczak, F. J., Richard, T. G. (2003c). Forces associated with pneumatic power screwdriver operation: statics and dynamics. Ergonomics, Vol. 46, No. 12, 1161-1177.

[21] Sesto, M. E., Chourasia, A. O., Block, W. F., Radwin, R. G. (2008). Mechanical and magnetic resonance imaging changes following eccentric or concentric exertions. Clin. Biomech., 23 (7) 961-968.

[22] Forsman, M., Cyren, H., Moller, T., Kadefors, R., Mathiassen, S. E. (2002). Activity in five muscles during joint securing using pneumatic nutrunners. International Journal of Industrial Ergonomics, 29, 21-32.

[23] McGorry, R. W., Maikala, R. V., Lin, J. H., Rivard, A. (2009). Oxygenation kinetics of forearm muscles as a function of handle diameter during a repetitive power grip force task. International Journal of Industrial Ergonomics, 39, 465-470.

[24] Sesto, M. E., Radwin, R. G., Block, W. F. (2005). Anatomical and mechanical changes following repetitive eccentric exertions. Clinical Biomechanics, 20, 41-49.

[25] Chang, C., Wang, M. J. (2001). Evaluating the effects of activation mode, torque and horizontal operating distance on hand-arm response while operating pneumatic screwdrivers. International Journal of Industrial Ergonomics, 28, 171-179.

[26] Kihlberg, S., Lindbeck, L. (1994). Pneumatic tool torque reactions. Applied Ergonomics, 25 (4), 242-247.

[27] Chang, C., Wang, M. J., Lin, S. (1999). Evaluating the effects of wearing gloves and wrist support on hand-arm response while operating an in-line pneumatic screwdriver. International Journal of Industrial Ergonomics, 24, 473-481.

[28] Chang, C., Wang, M. J. (2000). Evaluating factors that influence hand-arm stress while operating an electric screwdriver. Applied Ergonomics, 31, 283-289.

[29] Morgan, D. L., Proske, U. (2004). Popping sarcomere hypothesis explains stretch induced muscle damage. Proceedings of the Australian physiological and pharmacological society, 34: 19-23.

[30] Ay, H., Luscher, A., Sommerich, C. (2017). A dynamic simulator for the ergonomics evaluation of powered torque tools for human assembly. Assembly Automation, Vol. 37, No. 1, 1-12.

[31] Abdel-Malek, D. M., Foley, R. C. A., Wakeely, F., Graham, J. D., Delfa, N. J. L. (2020). Exploring localized muscle fatigue responses at current upper-extremity ergonomics threshold limit values. Human Factors.

[32] Loewen, D., (2019). Design and evaluation of grasp assistive devices in an industrial environment. Master Thesis, Mechanical and Mechatronics Engineering, University of Waterloo.

[33] Winter, D. A., (2009). Biomechanics and motor control of human movement. Fourth Edition.

[34] Morgan, D. L., Proske, U. (2004). Popping sarcomere hypothesis explains stretch induced muscle damage. Proceedings of the Australian physiological and pharmacological society, 34: 19-23.

[35] Ay, H., (2011). Linear and nonlinear models of human hand-arm dynamics and torque tool interaction. Dissertation, The Ohio State University.

[36] Bakker, R., Kalra, M., Tomescu, S. S., Bahensky, R., Chandrashekar, N. (2022). The effects of pistol grip power tools on median nerve pressure and tendon strains. International Journal of Occupational Safety and Ergonomics, 28:3, 1904-1910.

[37] RSI and tool usage. https://app.croneri.co.uk/feature-articles/rsi-and-tool-usage. [Accessed on 10-11-2022].

[38] Hansen, J. T., (2014). Netter's clinical anatomy. 3rd Edition, Elsevier.

Appendices

Appendix A – Matlab Script

```
%% CODE INFO
%
% AUTHOR : RAJ ARJUN
% Last Updated: 14-10-2022

%% START

clc
clear all
tic
% format

%% ANTHROPOMETRIC & FILE DATA

tprompt = "Enter the torque (5, 7.5, 10) = ";
itorque = input(tprompt);

nprompt = "Enter the trial no. (1, 2, 3) = ";
trial = input(nprompt);

iprompt = "Enter the file name ('S1_1.xlsx', 'S2_1.xlsx', etc.) = ";
filename = input(iprompt);

oprompt = "Enter the output file name ('S1_R.xlsx', 'S2_R.xlsx') = ";
wfilename = input(oprompt);

if itorque == 5
    torque = '5';
else if itorque == 7.5
        torque = '7.5';
else if itorque == 10
        torque = '10';
end
end
end

file = xlsread(filename,torque);                        % file name

bodywt = xlsread(filename, torque, 'J6');               % body weight
(kg) - lab scale measured
mhand = 0.006*(bodywt);                                 % hand mass
(kg) - Dempster's relation
```

```
Jtool = 0.0013;                                          % MMOI tool -
averaged (=(Jtool1 + Jtool2)/2)
Jcable = 0.008928;                                       % MMOI tool-
cable - kgm^2
mcp = xlsread(filename, torque, 'J9');                   % 3rd MCP (cm)
- scale measured
% h = 0.025 + (mcp/100);                                 %
torque/moment arm length (m)
h = 0.09;                                                %
torque/moment arm length (m)
Jhand = (mhand)*(h^2);                                   % MMOI hand
(kgm^2)
MOI = Jtool + Jcable + Jhand;                            % Total MMOI
of tool+subject (kgm^2)

%% READ DATA FROM FILE

Alo = file(:,1);                % A LOW
Tlo = file(:,2);                % T LOW
Ahi = file(:,3);                % A HIGH
Thi = file(:,4);                % T HIGH
Aun = file(:,5);                % A UNDER
Tun = file(:,6);                % T UNDER
Ari = file(:,7);                % A RIGHT
Tri = file(:,8);                % T RIGHT

% Convert deg to radians
Alo = Alo*(pi/180);
Ahi = Ahi*(pi/180);
Aun = Aun*(pi/180);
Ari = Ari*(pi/180);

% Select Torque build up data (remove initial part with 'xx')
% prompt = "Enter the % cut-off for initial data = ";
% inital cutoff percentage
% cutper = input(prompt);
cutper = 20;
cutper = cutper/100;
mTlo = find(Tlo==max(Tlo));     % LO
xxlo = round(cutper*mTlo);      % no. of initial data points to
remove/delete
Tlo = Tlo(xxlo:mTlo);
nTlo = size(Tlo)+(xxlo-1);
Alo = Alo(xxlo:nTlo);
mThi = find(Thi==max(Thi));     % HI
xxhi = round(cutper*mThi);
Thi = Thi(xxhi:mThi);
nThi = size(Thi)+(xxhi-1);
Ahi = Ahi(xxhi:nThi);
mTun = find(Tun==max(Tun));     % UN
xxun = round(cutper*mTun);
Tun = Tun(xxun:mTun);
```

```
nTun = size(Tun)+(xxun-1);
Aun = Aun(xxun:nTun);
mTri = find(Tri==max(Tri));     % RI
xxri = round(cutper*mTri);
Tri = Tri(xxri:mTri);
nTri = size(Tri)+(xxri-1);
Ari = Ari(xxri:nTri);

% Sampling rate and sample size
sf = 1000;                      % sampling frequency (Hz)
t = 1/sf;
nlo = size(Alo,1);
nhi = size(Ahi,1);
nun = size(Aun,1);
nri = size(Ari,1);

% Filter - Angle or Torque
or = 2;
fc = 100;                       % cut-off freq
fs = 1000;                      % sampling rate
Wn = fc/(fs*0.5);
[BB,AA] = butter(or,Wn);        % low-pass Butterworth filter
Alo = filtfilt(BB,AA,Alo);      % Angle Filter
Ahi = filtfilt(BB,AA,Ahi);
Aun = filtfilt(BB,AA,Aun);
Ari = filtfilt(BB,AA,Ari);

%% ANGULAR VELOCITY

Avlo(1,1) = 0;
Avlo(nlo,1) = 0;
ii = 2;
while ii < nlo
    Avlo(ii) = (Alo(ii+1) - Alo(ii-1)) / (2*t);
    ii = ii + 1;
end
Avhi(1,1) = 0;
Avhi(nhi,1) = 0;
ii = 2;
while ii < nhi
    Avhi(ii) = (Ahi(ii+1) - Ahi(ii-1)) / (2*t);
    ii = ii + 1;
end
Avun(1,1) = 0;
Avun(nun,1) = 0;
ii = 2;
while ii < nun
    Avun(ii) = (Aun(ii+1) - Aun(ii-1)) / (2*t);
    ii = ii + 1;
end
Avri(1,1) = 0;
Avri(nri,1) = 0;
```

```
ii = 2;
while ii < nri
    Avri(ii) = (Ari(ii+1) - Ari(ii-1)) / (2*t);
    ii = ii + 1;
end

%% ANGULAR ACCELERATION

Aalo(1,1) = 0;
Aalo(2,1) = 0;
Aalo(nlo-1,1) = 0;
Aalo(nlo,1) = 0;
ii = 2;
while ii < nlo-1
    Aalo(ii,1) = (Avlo(ii+1,1) - Avlo(ii-1,1)) / (2*t);
    ii = ii+1;
end
Aahi(1,1) = 0;
Aahi(2,1) = 0;
Aahi(nhi-1,1) = 0;
Aahi(nhi,1) = 0;
ii = 2;
while ii < nhi-1
    Aahi(ii,1) = (Avhi(ii+1,1) - Avhi(ii-1,1)) / (2*t);
    ii = ii+1;
end
Aaun(1,1) = 0;
Aaun(2,1) = 0;
Aaun(nun-1,1) = 0;
Aaun(nun,1) = 0;
ii = 2;
while ii < nun-1
    Aaun(ii,1) = (Avun(ii+1,1) - Avun(ii-1,1)) / (2*t);
    ii = ii+1;
end
Aari(1,1) = 0;
Aari(2,1) = 0;
Aari(nri-1,1) = 0;
Aari(nri,1) = 0;
ii = 2;
while ii < nri-1
    Aari(ii,1) = (Avri(ii+1,1) - Avri(ii-1,1)) / (2*t);
    ii = ii+1;
end

Avlo(1) = NaN;  Avlo(2) = NaN;  Avlo(nlo) = NaN;
Avhi(1) = NaN;  Avhi(2) = NaN;  Avhi(nhi) = NaN;
Avun(1) = NaN;  Avun(2) = NaN;  Avun(nun) = NaN;
Avri(1) = NaN;  Avri(2) = NaN;  Avri(nri) = NaN;
Aalo(1) = NaN;  Aalo(2) = NaN;  Aalo(3) = NaN;  Aalo(nlo) = NaN;
Aahi(1) = NaN;  Aahi(2) = NaN;  Aahi(3) = NaN;  Aahi(nhi) = NaN;
Aaun(1) = NaN;  Aaun(2) = NaN;  Aaun(3) = NaN;  Aaun(nun) = NaN;
```

```
Aari(1) = NaN;  Aari(2) = NaN;  Aari(3) = NaN;  Aari(nri) = NaN;

%% EQUATION OF MOTION / MODEL

Lhslo = (Tlo - (MOI*Aalo));         % LO
Rhslo = [Alo Avlo];
KClo = Lhslo./Rhslo;
Klo = KClo(:,1);  Clo = KClo(:,2);  % Stiffness & Damping matrix
Lhshi = (Thi - (MOI*Aahi));         % HI
Rhshi = [Ahi Avhi];
KChi = Lhshi./Rhshi;
Khi = KChi(:,1);  Chi = KChi(:,2);
Lhsun = (Tun - (MOI*Aaun));         % UN
Rhsun = [Aun Avun];
KCun = Lhsun./Rhsun;
Kun = KCun(:,1);  Cun = KCun(:,2);
Lhsri = (Tri - (MOI*Aari));         % RI
Rhsri = [Ari Avri];
KCri = Lhsri./Rhsri;
Kri = KCri(:,1);  Cri = KCri(:,2);

% Divide moment arm length
klo = Klo/(h^2);  clo = Clo/(h^2);
khi = Khi/(h^2);  chi = Chi/(h^2);
kun = Kun/(h^2);  cun = Cun/(h^2);
kri = Kri/(h^2);  cri = Cri/(h^2);

% Average of K and C

nklo = klo(4:(size(klo,1)-1));      % K LO
avgKlo = mean(nklo);
sizeKlo = round(size(klo));
sizeKlo = sizeKlo(:,1);
aKlo = zeros(sizeKlo,1) + avgKlo;
nclo = clo(4:(size(clo,1)-1));      % C LO
avgClo = mean(nclo);
sizeClo = round(size(clo));
sizeClo = sizeClo(:,1);
aClo = zeros(sizeClo,1) + avgClo;

nkhi = khi(4:(size(khi,1)-1));      % K HI
avgKhi = mean(nkhi);
sizeKhi = round(size(khi));
sizeKhi = sizeKhi(:,1);
aKhi = zeros(sizeKhi,1) + avgKhi;
nchi = chi(4:(size(chi,1)-1));      % C HI
avgChi = mean(nchi);
sizeChi = round(size(chi));
sizeChi = sizeChi(:,1);
aChi = zeros(sizeChi,1) + avgChi;

nkun = kun(4:(size(kun,1)-1));      % K UN
```

```
avgKun = mean(nkun);
sizeKun = round(size(kun));
sizeKun = sizeKun(:,1);
aKun = zeros(sizeKun,1) + avgKun;
ncun = cun(4:(size(cun,1)-1));      % C UN
avgCun = mean(ncun);
sizeCun = round(size(cun));
sizeCun = sizeCun(:,1);
aCun = zeros(sizeCun,1) + avgCun;

nkri = kri(4:(size(kri,1)-1));      % K RI
avgKri = mean(nkri);
sizeKri = round(size(kri));
sizeKri = sizeKri(:,1);
aKri = zeros(sizeKri,1) + avgKri;
ncri = cri(4:(size(cri,1)-1));      % C RI
avgCri = mean(ncri);
sizeCri = round(size(cri));
sizeCri = sizeCri(:,1);
aCri = zeros(sizeCri,1) + avgCri;

%% PLOTS

figure(1)                   % Torque, Angle, Vel, Acc plots
subplot(4,1,1)
plot(Tlo, 'b')
hold on
plot(Thi, 'g')
hold on
plot(Tun, 'r')
hold on
plot(Tri, 'k')
title('Torque (Nm)')
legend('Low', 'High', 'Under', 'Right')
subplot(4,1,2)
plot(Alo, 'b')
hold on
plot(Ahi, 'g')
hold on
plot(Aun, 'r')
hold on
plot(Ari, 'k')
title('Angle (rad)')
subplot(4,1,3)
plot(Avlo, 'b')
hold on
plot(Avhi, 'g')
hold on
plot(Avun, 'r')
hold on
plot(Avri, 'k')
title('Angular velocity (rad/s)')
```

```
subplot(4,1,4)
plot(Aalo, 'b')
hold on
plot(Aahi, 'g')
hold on
plot(Aaun, 'r')
hold on
plot(Aari, 'k')
title('Angular acceleration (rad/s^2)')

figure(2)                    % Stiffness, Damping plots
subplot(2,1,1)
plot(klo, 'b')
hold on
plot(khi, 'g')
hold on
plot(kun, 'r')
hold on
plot(kri, 'k')
hold on
plot(aKlo, 'b')
hold on
plot(aKhi, 'g')
hold on
plot(aKun, 'r')
hold on
plot(aKri, 'k')
title('Stiffness (N/m)')
legend('Low', 'High', 'Under', 'Right')
subplot(2,1,2)
plot(clo, 'b')
hold on
plot(chi, 'g')
hold on
plot(cun, 'r')
hold on
plot(cri, 'k')
hold on
plot(aClo, 'b')
hold on
plot(aChi, 'g')
hold on
plot(aCun, 'r')
hold on
plot(aCri, 'k')
title('Damping (Ns/m)')

%% AIR CYLINDER PRESSURE

Strokefull = 8*0.0254;
Strokehalf = Strokefull/2;
Bdia = (7/16)*0.0254;
```

```
Rdia = 0.19*0.0254;
RArea = (pi*Rdia*Rdia)/4;
BArea = (pi*Bdia*Bdia)/4;
EffArea = BArea-RArea;
Volex = BArea*Strokehalf;
Volin = Volex + (EffArea*Strokehalf);
Pascal = 0.0001450377;

Pconstant = (Volin*Pascal)/(2*EffArea*EffArea);
kinherent = 519.6278;
Pratio = (EffArea*Strokehalf)/Volex;

Pinlo = Pconstant*(klo-kinherent);
nPinlo = Pinlo(4:(size(Pinlo,1)-1));
aPinlo = mean(nPinlo);
sizenPinlo = round(size(nPinlo));
sizenPinlo = sizenPinlo(:,1);
aPinlo = zeros(sizenPinlo,1) + aPinlo;

Pinhi = Pconstant*(khi-kinherent);
nPinhi = Pinhi(4:(size(Pinhi,1)-1));
aPinhi = mean(nPinhi);
sizenPinhi = round(size(nPinhi));
sizenPinhi = sizenPinhi(:,1);
aPinhi = zeros(sizenPinhi,1) + aPinhi;

Pinun = Pconstant*(kun-kinherent);
nPinun = Pinun(4:(size(Pinun,1)-1));
aPinun = mean(nPinun);
sizenPinun = round(size(nPinun));
sizenPinun = sizenPinun(:,1);
aPinun = zeros(sizenPinun,1) + aPinun;

Pinri = Pconstant*(kri-kinherent);
nPinri = Pinri(4:(size(Pinri,1)-1));
aPinri = mean(nPinri);
sizenPinri = round(size(nPinri));
sizenPinri = sizenPinri(:,1);
aPinri = zeros(sizenPinri,1) + aPinri;

% Pressure Plot
figure(3)
plot(Pinlo, 'b')
hold on
plot(Pinhi, 'g')
hold on
plot(Pinun, 'r')
hold on
plot(Pinri, 'k')
hold on
plot(aPinlo,'b')
hold on
```

```
plot(aPinhi,'g')
hold on
plot(aPinun,'r')
hold on
plot(aPinri,'k')
title('Cylinder pressure')
xlabel('time, ms')
ylabel('psi')
legend('Low', 'High', 'Under', 'Right')

%% PRINT VALUES

% Percentile K & C [10, 50, 90]

klo10 = prctile(nklo,10);           % K LO
klo50 = prctile(nklo,50);
klo90 = prctile(nklo,90);
clo10 = prctile(nclo,10);           % K LO
clo50 = prctile(nclo,50);
clo90 = prctile(nclo,90);
khi10 = prctile(nkhi,10);           % K HI
khi50 = prctile(nkhi,50);
khi90 = prctile(nkhi,90);
chi10 = prctile(nchi,10);           % C HI
chi50 = prctile(nchi,50);
chi90 = prctile(nchi,90);
kun10 = prctile(nkun,10);           % K UN
kun50 = prctile(nkun,50);
kun90 = prctile(nkun,90);
cun10 = prctile(ncun,10);           % C UN
cun50 = prctile(ncun,50);
cun90 = prctile(ncun,90);
kri10 = prctile(nkri,10);           % K RI
kri50 = prctile(nkri,50);
kri90 = prctile(nkri,90);
cri10 = prctile(ncri,10);           % C RI
cri50 = prctile(ncri,50);
cri90 = prctile(ncri,90);

% T,A,K,C Print Values
T_LO = max(Tlo);
T_HI = max(Thi);
T_UN = max(Tun);
T_RI = max(Tri);
A_LO = max(Alo)*(180/pi);
A_HI = max(Ahi)*(180/pi);
A_UN = max(Aun)*(180/pi);
A_RI = max(Ari)*(180/pi);
K_LO = max(aKlo);
K_HI = max(aKhi);
K_UN = max(aKun);
K_RI = max(aKri);
```

```
C_LO = max(aClo);
C_HI = max(aChi);
C_UN = max(aCun);
C_RI = max(aCri);

% Pressure Print Values
P_LO = aPinlo(1,:);
P_HI = aPinhi(1,:);
P_UN = aPinun(1,:);
P_RI = aPinri(1,:);
Plo10 = prctile(nPinlo,10);           % P LO
Plo50 = prctile(nPinlo,50);
Plo90 = prctile(nPinlo,90);
Phi10 = prctile(nPinhi,10);           % P HI
Phi50 = prctile(nPinhi,50);
Phi90 = prctile(nPinhi,90);
Pun10 = prctile(nPinun,10);           % P UN
Pun50 = prctile(nPinun,50);
Pun90 = prctile(nPinun,90);
Pri10 = prctile(nPinri,10);           % P RI
Pri50 = prctile(nPinri,50);
Pri90 = prctile(nPinri,90);

% P2
P80_LO = Pratio*(max(aPinlo));
P80_HI = Pratio*(max(aPinhi));
P80_UN = Pratio*(max(aPinun));
P80_RI = Pratio*(max(aPinri));

% TABLE 1
VALUE1 = {'Max T';'Max A';' ';'Avg K';'10% K';'50% K';'90% K';' ';'Avg
C';'10% C';'50% C';'90% C';' ';'10% P';'50% P';'90% P';'2nd P';'Avg
P'};
LOW1 = [T_LO; A_LO; nan; K_LO; klo10; klo50; klo90; nan; C_LO; clo10;
clo50; clo90; nan; Plo10; Plo50; Plo90; P80_LO; P_LO];
HIGH1 = [T_HI; A_HI; nan; K_HI; khi10; khi50; khi90; nan; C_HI; chi10;
chi50; chi90; nan; Phi10; Phi50; Phi90; P80_HI; P_HI];
UNDER1 = [T_UN; A_UN; nan; K_UN; kun10; kun50; kun90; nan; C_UN;
cun10; cun50; cun90; nan; Pun10; Pun50; Pun90; P80_UN; P_UN];
RIGHT1 = [T_RI; A_RI; nan; K_RI; kri10; kri50; kri90; nan; C_RI;
cri10; cri50; cun90; nan; Pri10; Pri50; Pri90; P80_RI; P_RI];
T1 = table(VALUE1, LOW1, HIGH1, UNDER1, RIGHT1)

% TABLE 2
VALUE = {'Max T';'Max A';'Avg K';'10% K';'50% K';'90% K';'Avg C';'10%
C';'50% C';'90% C';'10% P';'50% P';'90% P';'2nd P';'Avg P'};
LOW = [T_LO; A_LO; K_LO; klo10; klo50; klo90; C_LO; clo10; clo50;
clo90; Plo10; Plo50; Plo90; P80_LO; P_LO];
HIGH = [T_HI; A_HI; K_HI; khi10; khi50; khi90; C_HI; chi10; chi50;
chi90; Phi10; Phi50; Phi90; P80_HI; P_HI];
UNDER = [T_UN; A_UN; K_UN; kun10; kun50; kun90; C_UN; cun10; cun50;
cun90; Pun10; Pun50; Pun90; P80_UN; P_UN];
```

```
RIGHT = [T_RI; A_RI; K_RI; kri10; kri50; kri90; C_RI; cri10; cri50;
cun90; Pri10; Pri50; Pri90; P80_RI; P_RI];
T2 = table(VALUE, LOW, HIGH, UNDER, RIGHT);

%% EXPORT DATA (Table 2) to OUTPUT FILE

if itorque == 5
    wnt = 1;
else if itorque == 7.5
        wnt = 2;
else if itorque == 10
        wnt = 3;
end
end
end

if trial == 1
    writetable(T2, wfilename, 'Sheet', wnt, 'Range', 'A1:E16')
else if trial == 2
        writetable(T2, wfilename, 'Sheet', wnt, 'Range', 'A18:E33')
else if trial == 3
        writetable(T2, wfilename, 'Sheet', wnt, 'Range', 'A35:E50')
end
end
end

%% END OF CODE

toc
```

Appendix B – Reference Table

Author, Year	Method	Independent variables	Dependent variables	Muscles studied	Tool types	Reaction parameters
Lin, 2001	Mathematical model	Work locations, gender	Stiffness, damping, handle displacement	-	PG	Handle displacement, hand force
Lin, 2003a	Mathematical model	Work locations, tool shapes, orientation	Stiffness, damping, mass moment of inertia	-	IL, PG, RA	Stiffness
Lin, 2003b	Mathematical model, Physiological	Gender, work location, joint hardness	Stiffness, damping, handle displacement, hand force	Superficial lateral epicondyle	IL, PG, RA	Handle displacement, hand force
Lin, 2005	Mathematical model	Work locations, tool shapes, orientation	Handle displacement	-	IL, PG, RA	Handle displacement
Lin, 2007a	Physiological measure	Operator experience, joint hardness, work location	Average EMG	Forearm flexors, extensor, biceps	PG, RA	Grip force, handle displacement
Ku, 2007	Experimental	Tool properties, fasteners, orientation, work location	Handle force, handle displacement	-	PG, RA	Hand force, handle displacement
Lin, 2010a	Physiological measure	Work location, tool type	Grip force (EMG)	Forearm digitorum superficialis, extensor digitorum communis, upper trapezius	PG, RA	Grip force
Lin, 2007b	Experimental	Tool type, joint hardness	Grip force, hand moment	-	PG, RA, IL	Grip force, hand moment
Kihlberg, 1995	Subjective rating	Joint hardness, tool torque, shut-off mechanism	Subjective ratings, torque impulse	-	N/A	Torque impulse

Lin, 2010b	Physiological measure	Work:rest pattern, torque, task pace	Tissue oxygenation, blood volume (NIRS)	Forearm digitorum superficialis, extensor digitorum communis	PG	Grip force
Steingraber, 2021	Physiological measure	Tightening strategy, orientation, torque, joint hardness	Force impulse, handle displacement, EMG magnitude	PM, UT, AD, BB, TB, FCU, FCR, ECU	RA	Force impulse, handle displacement
Kihlberg, 1993	Physiological measure, subjective rating	Shut-off mechanism	Reaction force, displacement, muscle activity (EMG), discomfort rating	Arm, shoulder	RA	Reaction force, handle displacement
Lin, 2008	Subjective rating	Work location, torque, joint hardness, handle length, tool type	Subjective ratings	-	PG, RA	Discomfort rating
Lin, 2012	Physiological measure, subjective rating	Joint hardness, work:rest pattern, task pace	Grip force (%MVE), perceived exertions	N/A	PG	Grip force
Ay, 2010	Experimental simulation	Torque, joint hardness, operator dynamic properties	Handle displacement, hand force, acceptance rating	-	RA	Handle displacement, hand force